Room temperature Planar Hall effect in nanostructures of trigonal-PtBi$_2$
Response to referees, round #2

REPORT #2, REFEREE 1 (SAME AS REPORT #2 OF FIRST ROUND)

Report

I appreciate the authors' response to my technical queries, but I am not convinced by their response to some of the conceptual questions. To my understanding, the main claims of this manuscript include: i) the observation of the planar Hall effect up to room temperature; ii) experimental evidence of the impact of band topology on the electronic transport ("Our results strengthen the topological nature of PtBi2 and the strong influence of quantum geometric effects on the electronic transport...")

Regarding i), another reviewer has already raised some technical concerns that have to be addressed. My main doubts concern the point ii), as follows:

We want to thank the reviewer for their once again very thorough review. We have addressed the technical concerns regarding the observation of the PHE in the response to the other review. In this response, we focus on the questions raised as to ii) and the experimental evidence of the impact of the Weyl topology on the transport.

First, we would like to point out that, in our opinion, it is impossible to completely lift the ambiguity associated with the attribution of the observed effects to the non-trivial topology of t-PtBi2. At best, we can show that the data is consistent with the theoretical prediction, and we can show that some other effects cannot be at the origin of the effects observed. This is what we claim in the manuscript (i.e. "Our results strengthen..." and not e.g. "Our results demonstrate").

1. Fig. 1 depicting 12 Weyl nodes has been added to the manuscript. However, other Weyl nodes are still prominently mentioned in the discussion. Some of them lie very far away from the Fermi level (-655 meV, -497 meV), and it is very hard to imagine that such features may contribute to the transport, so I am not sure why they are mentioned at all. It gets even more confusing with the last added sentence in the first paragraph of the Discussion: "...these 6 groups are referred to as the field-generated Weyl nodes, as they exist even in the absence of an external magnetic field". It's probably a typo, and the authors imply that these nodes appear in the magnetic field only. But on reading this paragraph several times I am still not quite sure what the intended meaning is. The whole discussion of these "distant" Weyl nodes is very obscure and seemingly irrelevant to the experimental data presented in this work, especially if APHE is excluded.

Regarding the field-generated Weyl nodes, this is indeed a typo, and we thank the reviewer for pointing it out! This has been corrected in the new version of the manuscript (this part has been moved to the SM). It now reads: "In the folowing, these 6 groups are refered to as the "field-generated" Weyl nodes, as they only appear when an external magnetic field is applied".

We agree that the numerous groups of Weyl nodes have made our point less clear in the discussion of which Weyl nodes would contribute the most to the PHE, and we have adressed this in the new version of the manuscript. The point of this paper is to show that an effect which would be expected in a Weyl semimetals (with the 12 Weyl nodes closest to the Fermi level) is indeed being observed. We agree that the Weyl nodes with the largest contribution to the PHE are most likely the 12 closest to E$_F$, and have shifted the discussion about the different arguments related to the other Weyl nodes to the SM.

2. Different calculations of the Fermi surface (Fig. 8c in PRM'2020; Fig. 1c in Nature'2024; Fig. 5 in arXiv:2504.13661) all show large sheets that lie somewhat far away from the anticipated Weyl nodes shown in Fig. 1 of the present work. What is the rationale for discussing electronic transport in the context of these Weyl nodes? What about the large and "conventional" parts of the Fermi surface that should, naively, dominate the transport?

The Fermi surface is made up of sheets from multiple bands, one of which (band 48) hosts the Weyl points shown in figure 1. On the other hand, the PHE can have different origins, such as intrinsic magnetism, anisotropic orbital magnetoresistance (AOMR), and Weyl topology. Without one of these specific properties, no PHE is expected. Given

that t-PtBi$_2$ is non magnetic, the main origins for the PHE left are AOMR and Weyl topology, between which there are no clear-cut ways to distinguish. In this manuscript, we simply state that the measurements are entirely consistent with the prediction and other observations (from multiple other techniques) of Weyl topology in the material. As stated in the paragraph prefacing this response, we do not believe any transport experiment one may carry will be able to fully demonstrate the topological origin of the effect (when no clear chiral anomaly is visible, at least). Instead, successive studies from different methods can raise the likeliness of this origin.

Regarding the conventional part of the Fermi surface, they indeed do dominate the transport properties, as seen by the large average longitudinal resistance (typically 1 Ω) around which the signal oscillates (by at most 100 mΩ).

3. A concurrent study of the planar Hall effect in PtBi2 has been published by Zhu et al. [PRB 110, 125148 (2024)]. It appeared in September 2024, about a month before the initial submission and half a year before the resubmission of the present manuscript, yet it has not been mentioned at all. Detailed transport measurements are certainly time-consuming, and the publication of similar data by another group does not compromise the novelty per se. However, it does raise some conceptual questions about the interpretation, because Zhu et al. arrive at a very different conclusion that the properties of the PtBi2 flakes are dominated by anisotropic orbital magnetoresistance. In fact, that study looks more convincing because it juxtaposes transport measurements on the bulk samples and thin flakes, and eventually identifies the possible effects of band topology in the bulk but not in the flakes. It also shows a direct comparison of the RRR of the bulk and thin-flake samples and demonstrates a quite drastic reduction in the sample quality (in terms of RRR) upon exfoliation. While a similar reduction in RRR can be inferred from the authors' response, it does not appear prominently in the manuscript, although it seems crucial for the interpretation, especially with the knowledge that bulk samples show a much stronger resemblance to the expected behavior of a Weyl semi-metal than the thin flakes.

As a peer, I find it confusing and even disconcerting that similar data are used to produce entirely different claims: orbital magnetoresistance by Zhu et al. vs. "quantum geometric effects" in the present work. In my opinion, the authors should either find an interpretation consistent with Zhu et al., or provide clear-cut arguments why their data unambiguously prove the role of band topology in the electronic transport. Otherwise, this work will mainly generate confusion instead of clarifying the physics of the potentially interesting quantum material.

We only became aware of the Zhu et al. publication after the initial submission of this manuscript. We thank the reviewer for giving us the possibility to include a discussion of these results in the current version of the manuscript. In our humble opinion, the publication by Zhu et al. does not invalidate our study, as there are strong differences between our study and the Zhu et al. publication:

➤ In our study, we show the full temperature dependence of the PHE for nanostructures (only base temperature is shown in Zhu et al.), showing that the PHE persists even at room temperature. While we cannot compare with the nanostructures of Zhu et al., we note that our temperature dependence is completely different from the one they show for bulk.

➤ In our study, we reach higher magnetic fields (14T instead of 9T), and still do not see any evidence of large "kinks" in the data (which they see around 45° and 90°), which they attribute to an "abnormal PHE" with band structure symmetry origin (though completely distinct from the APHE we reported on previously), with seemingly a $\pi/2$ periodicity (of which we find no evidence in our measurements, see the APHE publication)

➤ We find a different field dependence, $\Delta\rho \propto 1.24$, showing a clear non-linearity compared to their data ($\Delta\rho_{xx} \propto 1.15$ and $\Delta\rho_{yx} \propto 1.05$, although we are unsure as to how to explain such a large difference between the two axes).

➤ We feature a much more in-depth analysis of the data, merging the analysis of ρ_{xx} and ρ_{yx} (as is the case in the theory), and discussing in details the deviations from the simple theory model.

➤ We offer reproducibility, with 3 samples showing the same effect at low fields, 2 of which were measured at higher fields and still show the same effect, compared to (seemingly, as they don't show the pictures of the actual samples) 1 bulk crystal and 1 nanostructure in Zhu et al.

➤ As mentioned previously, the differences in DFT calculations between our two groups seems to indicate a small difference in the crystal structure (while presumably preserving symmetries), resulting in potentially massive differences in the band structure.

We therefore strongly believe that our study of this effect significantly furthers the knowledge on the PHE in PtBi$_2$, despite the results of Zhu et al.

Beyond those arguments, we also point out that we have certain concerns about the data presented in Zhu et al. One of our major concerns being that while the publication ostensibly presents measurements over the entire 0°-360° angular range, the data seems to be (anti)symmetrized from the 0°-90° range, therefore assuming the PHE symmetries from the get-go and biasing the rest of the study.

Additionally, I would like to mention that I find it rather disturbing when different pieces of characterization are scattered across different publications. Readers are sent to Ref. 19 to see temperature dependence of the resistivity and RRR, and to the supplemental material of the Nano Lett.'2023 publication to see the effect of the contacts geometry. It is at best inconvenient. Moreover, some of the most exciting results for PtBi2 demonstrate an acute sample dependence, see the very unsystematic superconducting gaps shown in the STM study [Nature Comm. 15, 9895 (2024)] and the absence of superconductivity in arXiv:2503.08841, as opposed to Nature'2024, etc. While I understand that these different Dresden-centered publications on PtBi2 are related to different collaborators, I have to say that there are growing doubts on whether all unconventional and exciting physics of PtBi2 is really intrinsic. Careful tracking of the sample characterization and comparisons between the bulk and thin-flake samples could help to resolve these doubts.

We agree with the reviewer that the transport characterization information on the material is somewhat scattered in different articles from different journals, which is unfortunate. Given that this study pertains to a specific analysis on a measurement campaign shared with Ref. 19, and on samples shared with Ref. 19 and the 2023 Nano Lett. publication, we reproduce in (the supplemental material of) this manuscript the relevant data.

Regarding the variability of the results on t-PtBi$_2$, it seems less related to sample dependence than to growth dependence: arXiv:2503.08841 and Zhu et al. [PRB 110, 125148 (2024)] each grew their own crystals, which seem to have different properties than those grown in Dresden, which would indeed deserve further research, but is beyond the scope of this study. If the surface state properties appear to be relatively fragile and very sensitive to any contamination, there is a very strong reproducibility of the bulk properties and transport data. We have now grown dozens of crystals whose quality (in terms of RRR) may vary but which, once exfoliated, all show similar properties (superconductivity with similar Tc/Bc, PHE, APHE in ref 19., MR). From these crystals onward, the decrease in RRR due to exfoliation is, for example, systematic and highly predictable, and is accompanied by an equally systematic decrease in magnetoresistance. Above all, as far as the subject of this work is concerned, PHE is an extremely stable and reproducible effect. Finally, measurements taken by others and notably the group of Zhu et al. publication also show very comparable raw data. The differences are essentially in the way we interpret them.

REPORT #1, REFEREE 3

Report

The authors have measured the transverse and the longitudinal resistance of three exfoliated samples of t-PtBi2 flakes in a magnetic field rotating the mutual orientation of applied current and magnetic field. The study produces interesting data and beautiful figures. However, this reviewer is not impressed by the analysis and the presentation and believes that it is not appropriate for Scipost. Here is the list of my objections.

We thank the reviewer for their input as to our manuscript. We believe we have answered their concerns below.

i) The main observation is that both longitudinal and transverse resistance oscillate with a periodicity of 180° and these oscillations are phase shifted. But this is a trivial result, expected in any metal. When the magnetic field and the electric current, there is a Lorentz force and when they are parallel, there is no Lorentz force. Independent of microscopic details. When the current and field are parallel to each other, the longitudinal resistance is expected to be lower than when they are perpendicular. When the current and field are parallel to each other, the transverse resistance is expected to be zero, provided that: i) There is no misalignment; ii) The symmetry axes of the crystal and the Fermi surface pockets coincide with each other. There is no discussion of these prosaic possibilities in this paper.

We are unsure if we understand the reviewer's argument correctly.
On the one hand, if the reviewer is referring to a "conventional" Hall effect, with both E and B fields in the plane, this would give a measurable effect in R_{zx}, and not R_{yx}. This would be challenging to measure, and we don't expect to see this effect in our geometry due to 1) the small thickness of our flakes and 2) the fact that our electrical contacts cover the entire sides of the flakes, from top to bottom.
On the other hand, the reviewer may be referring to a less trivial effect: even in our configuration, a Lorentz force would be expected to have some sort of influence on the (x-y) off-diagonal terms of the resistivity tensor, which would lead to a periodic signal in both R_{xx} and R_{yx}. However in this case, we would not expect the signal to be measurable in a non-magnetic material. In such materials, such periodic signals would more likely originate from current jetting effects, but in our case the magnetoresistance is too small for a sizable current jetting to occur, and the shapes of the nanostructure would also minimize this effect. Furthermore, this signal would still be akin to a "conventional" Hall effect, which is typically very weak in metals due to the large concentration of carriers (the Hall signal being inversely proportional to n), which would also imply that the signal would be too small to measure.
Finally, the argument presented by the reviewer is extremely broad, and should therefore be seen in most materials, which is simply not the case. The effect observed here has all the characteristics of the well-known planar Hall effect, an effect well-studied in magnetic [C. Wouters et al., Sensors and Actuators A: Physical, 237, 2016, 62-71] and strong-spin-orbit materials [Wadehra et al., Nat. Comm. 11, 874 (2020)] and expected in Weyl semimetals [Nandy et al., Phys. Rev. Lett. 119, 176804 (2017)].
A paragraph was added in the planar Hall effect section of the manuscript, to prevent misunderstandings from readers:
We note that, despite its historical name, the planar Hall effect is mostly a magnetism or band structure effect, and isn't typically linked to any Lorentz force from the (in-plane) magnetic field acting on the charge carriers.

ii) A serious study of transport in any metal (topological or otherwise) would inform the reader about the RRR of the samples, the mean free path (or the mobility) of electrons, the carrier density of the system, the shape and the anisotropy of the Fermi surface, before linking the results to any exotic physics, such as the presence of Weyl nodes. There is no trace of this here. The modest amplitude of the magnetoresistance indicates that low-temperature mobility is not very high.

The RRRs of all samples are shown in the Methods section. The mobility (or mobilities) in the samples is not known, as the magnetoresistance of the nanostructures does not show a simple Hall effect (i.e consistent with a e.g. 1- or 2-band model), which might be due to the large number of bands crossing the Fermi level (6). The carrier mobility nonetheless seems to be low, as Shobnikhov-de Haas oscillations in nanostructures start appearing only at rather high fields. This study of transport properties has been done in a previous publication [1], and is therefore only referenced in the current manuscript.

iii) The issue of reproducibility is not addressed (or rather addressed in a strange way). Yes, all three samples show phase-shifted oscillations of the conductivity. But this is trivial. Do the color figures of Fig.3d-i, become similar when the same angular convention (phi=0 when I//B) is used? Why not plot resistivity (and not resistance)? Is the amplitude of the oscillations in three samples identical in resistivity or conductivity? This looks unlikely. The relative size of oscillations in Rxx is 4e-3 in sample 19e-3 in sample 2, and 22e-3 in sample 3. Since sample 2 and 3 are those which have the most irregular shape, one wonders if the observed signal is not enhanced by them. The irreproducibility in the case of the Hall resistance is even larger. Even the sign of the effect is not the same across the three samples.

We answer the multiple points raised by the reviewer below.

- The mappings shown in figure 3 look qualitatively similar when rotated to account for the different current orientations in the three samples as it can be directly seen from the figure 3.

- As pointed out in the main text, extracting the resistivity from the resistance in samples which do not have perfect Hall bar geometries is highly non-trivial, and requires a complex fitting procedure to obtain. This was done for samples D1 and D2 in the higher field measurements, to extract the amplitude of the oscillations in resistivity.

- The resistivity is not the same between the three samples, nor is the amplitude of the oscillations in resistivity the same. We have no clear explanation for that but we note however that a detailed analysis can be rather complicated by the fact that the RRR is strongly thickness dependent (unexplained so far but also observed by other groups) and by the contribution of surface states.

- We are unable to understand the numbers provided by the reviewer for the amplitude of the oscillations (4e-3, 19e-3 or 9e-3, and 22e-3), as we find roughly 8e-3, 9e-3, and 6e-3. In any case, different exfoliated samples with different contact geometries are not expected to show the same resistivities, especially not in the transverse direction. Instead, the comparison should be made between the oscillations in R_{xx} and in R_{yx} in each individual samples.

- We do not understand the meaning of "sign" of the effect. If this refers to the value of the amplitude of the oscillations, $\Delta\rho$, then it is here always positive by construction. If this refers to the positive or negative average value of the transverse resistance, it is due to the misalignment of the contacts on the samples, which can give a positive or negative longitudinal contribution to transverse measurements depending on the geometry of the samples. This is a purely geometric effect and has no link to the PHE.

iv) There is no information about the in-plane orientation of the applied current respective to the crystal axes. Is it the same in the three samples?

The direction of the applied current in all three samples can be seen at the top of figure 3. To our knowledge, there is no experimental way to determine the crystal orientations of such nanostructures contacted on Si/SiO2 substrates but can nonetheless be infered as the preferential axes along which the crystals exfoliate (i.e. the "long" direction of the flakes). A parallel study on the same three samples (ref 19), evidencing a separate crystal axes-dependent effect, suggests that the "long" directions of the samples are indeed crystal axes.
We note that the PHE is theoretically entirely independent from crystal orientation, and instead only depends on the orientation of the current with respect to the magnetic field.

v) The main result appears in the title of the paper. Have the authors observed a planar Hall effect at room temperature? I am not convinced. One needs to exclude misalignment. Since the authors admit that the plane of rotation may not be the (electric field, charge current) plane, then the whole signal may be due to a combination of rotational misalignment and a genuine in-plane anisotropy of Fermi velocity. Only a two-axis rotational set-up can dissipate any ambiguity. The fact that the oscillations keep their phase from 1K to 300 K is actually an argument in favor of misalignment origin.

- We do not see how the combination of misalignment and Fermi velocity anisotropy suggested by the reviewer would result in π-periodic oscillations of the longitudinal and transverse resistances, with the same amplitude in resistivites, as observed and expected of a PHE. We note that the trigonal structure of t-PtBi2 considered here would imply a C3 symmetry of the Fermi velocity ($2\pi/3$ periodic), well distinct from the π-periodicity of the PHE measured here.

- The effects of planar misalignment has been taken into account in our analysis, as stated above. Such a misalignment would induce indeed a π-periodic signal in the longitudinal signal that can interfere with the PHE but it induces a 2π-periodic signal in the transverse voltage and is therefore well distinct from the π-periodic PHE. Therefore, the two signals can be in general easily disentangled.

- We fail to see how the constant phase at different temperatures is in favor of misalignment, as it is literally what is expected for a PHE. Quite the opposite: a significant shifting of the phase may actually be attributed to current jetting, as we discuss in the manuscript, and it's absence doesn't relate neither to misalignment effects nor to the PHE.

Recommendation

Reject

[1] A. Veyrat, V. Labracherie, D. L. Bashlakov, F. Caglieris, J. I. Facio, G. Shipunov, T. Charvin, R. Acharya, Y. Naidyuk, R. Giraud, J. van den Brink, B. Büchner, C. Hess, S. Aswartham, and J. Dufouleur, Nano Lett. 10.1021/acs.nanolett.2c04297 (2023).

Room temperature Planar Hall effect in nanostructures of trigonal-PtBi$_2$

Arthur Veyrat,[1, 2, 3, *] Klaus Koepernik,[1, 2] Louis Veyrat,[1, 2, 4] Grigory Shipunov,[1, 2]
Iryna Kovalchuk,[5, 1] Saicharan Aswartham,[1, 2] Jiang Qu,[1, 2] Ankit Kumar,[1, 2] Michele
Ceccardi,[6, 7] Federico Caglieris,[7] Nicolás Pérez Rodríguez,[1, 2] Romain Giraud,[1, 2, 8] Bernd
Büchner,[1, 2, 9] Jeroen van den Brink,[1, 2, 9] Carmine Ortix,[10, †] and Joseph Dufouleur[1, 2, 11, ‡]

[1]*Leibniz Institute for Solid State and Materials Research (IFW Dresden), Helmholtzstraße 20, D-01069 Dresden, Germany*
[2]*Würzburg-Dresden Cluster of Excellence ct.qmat, Dresden, Germany*
[3]*Laboratoire de Physique des Solides (LPS Orsay), 510 Rue André Rivière, 91400 Orsay, France*
[4]*CNRS, Laboratoire National des Champs Magnétiques Intenses, Université Grenoble-Alpes,
Université Toulouse 3, INSA-Toulouse, EMFL, 31400 Toulouse, France*
[5]*Kyiv Academic University, 03142 Kyiv, Ukraine*
[6]*Department of Physics, University of Genoa, 16146 Genoa, Italy*
[7]*CNR-SPIN Institute, 16152 Genoa, Italy*
[8]*Université Grenoble Alpes, CNRS, CEA, Grenoble-INP, Spintec, F-38000 Grenoble, France*
[9]*Department of Physics, TU Dresden, D-01062 Dresden, Germany*
[10]*Dipartimento di Fisica "E. R. Caianiello", Universitá di Salerno, IT-84084 Fisciano (SA), Italy*
[11]*Center for Transport and Devices, TU Dresden, D-01069 Dresden, Germany*

Trigonal-PtBi$_2$ has recently garnered significant interest as it exhibits unique superconducting topological surface states due to electron pairing on Fermi arcs connecting bulk Weyl nodes. Furthermore, topological nodal lines have been predicted in trigonal-PtBi$_2$, and their signature was measured in magnetotransport as a dissipationless, *i.e.* odd under a magnetic field reversal, anomalous planar Hall effect. Understanding the topological superconducting surface state in trigonal-PtBi$_2$ requires unravelling the intrinsic geometric properties of the normal state electronic wavefunctions and further studies of their hallmarks in charge transport characteristics are needed. In this work, we reveal the presence of a strong dissipative, *i.e.* even under a magnetic field reversal, planar Hall effect in PtBi$_2$ at low magnetic fields and up to room temperature. This robust response can be attributed to the presence of Weyl nodes close to the Fermi energy. While this effect generally follows the theoretical prediction for a planar Hall effect in a Weyl semi-metal, we show that it deviates from theoretical expectations at both low fields and high temperatures. We also discuss the origin of the PHE in our material, and the contributions of both the topological features in PtBi$_2$ and its possible trivial origin. Our results strengthen the topological nature of PtBi$_2$ and the strong influence of quantum geometric effects on the electronic transport properties of the low energy normal state.

INTRODUCTION

Topology is, together with superconductivity, one of the most striking macroscopic manifestation of the quantum nature of electrons in quantum materials. A consequence of the geometric properties of the wave function, from which topological properties arise, is the existence of the Berry curvature (BC): an emerging magnetic field in momentum space. In a Weyl semi-metal, the Weyl nodes act as sources and sinks of BC [1] and can lead to signatures in charge-transport experiments such as the planar Hall effect (PHE) [2–4]: the appearance under an external in-plane magnetic field of a transverse voltage dependent on the relative orientations of the current and magnetic field. The PHE is dissipative, i.e. it is symmetric in magnetic field and associated with an in-plane field-dependent longitudinal voltage called anisotropic magnetoresistance (AMR) [5]. However, mechanisms different from the BC such as intrinsic or orbital magnetism can also result in a dissipative PHE and AMR, making it an ambiguous signature of quantum geometric properties [6, 7].

Here, we study the PHE in magnetic field and temperature to find new insight on the quantum geometric properties in trigonal-PtBi$_2$: a non-magnetic Weyl- and nodal-line-metal which was recently reported in transport experiments to exhibit sub-Kelvin 2D-superconductivity and a BKT transition in nanostructures [8]. Scanning tunnelling spectroscopy (STS) studies in this compound have reported higher-temperature surface superconductivity [9], which was confirmed by angle-resolved photoemission spectroscopy (ARPES) to be intrinsically – and solely – generated by topological Fermi arcs [10] (The presence of Fermi arcs was also confirmed by STS measurements [11]). Cuts of the DFT calculated band structure through Weyl nodes, as well as the position of the nodes in the Brillouin zone, can be see in Figure 1. This makes t-PtBi$_2$ a very promising candidate for intrinsic topological superconductivity.

A thorough investigation of the transport signatures of topological degeneracies in t-PtBi$_2$ are however still

lacking. Here, we focus on the bulk properties of t-PtBi$_2$ nanostructures and report on a robust dissipative PHE from low magnetic fields and up to room temperature. These results are entirely coherent with the predicted Weyl nature of t-PtBi$_2$. We note that, in a complementary study based on the same raw data[12], we evidence and thourougly analysed another effect known as the anomalous PHE (APHE). This effect, which is two orders of magnitude weaker PHE than the PHE, does not originate from Weyl nodes already existing without external magnetic field, but rather from a conversion of topological nodal lines (which we also predict in that separate study) into very distant Weyl nodes (in k-space). Because of their different origin and different analysis required for both signals, as well as the fact the APHE constitutes but a small perturbation compared to the PHE signal, the two effects are studied separately in each study and the latter is simply ignored in the present study.

PLANAR HALL EFFECT

Planar Hall effect in Weyl Semi-metals

The planar Hall effect is a generic signature of the anisotropy of the magnetoresistivity that uniquely depends on the relative orientations of the in-plane magnetic field and electric field (i.e. current) in the sample. It thus corresponds to a difference $\Delta\sigma = \sigma_\parallel - \sigma_\perp$ between the conductivity $\sigma_\parallel$ when the two fields are aligned, and the conductivity $\sigma_\perp$ when they are orthogonal. As a result, it manifests itself both in transverse and longitudinal resistance measurements (the latter being sometimes referred to as anisotropic magnetoresistance, AMR, or anisotropic longitudinal magnetoconductance, LMC). Since the two effects (PHE and LMC/AMR) are in a one-to-one correspondence linked, we will refer to them both as PHE from here on. The planar Hall effect has historically been predicted and discovered in ferromagnets [13, 14], where the anisotropy is caused by the concomitant presence of intrinsic magnetization of the material and spin-orbit interaction. In materials without long-range magnetic order, a giant PHE has been predicted to occur in Dirac and Weyl semi-metals as a direct consequence of the chiral anomaly [2, 3]. This results in a large negative contribution to the longitudinal magnetoresistance when the magnetic and electric fields are aligned [2, 15]. In the simple case of a type-I Weyl cone (i.e. when the Weyl cone is not tilted), the contributions of the PHE to the longitudinal conductivity σ_{xx} and the transverse conductivity σ_{yx} follow the angular dependence [3]:

$$
\begin{aligned}
\sigma_{xx}^{PHE}(\varphi) &= \sigma_\perp + \Delta\sigma \, \cos^2\varphi, \\
\sigma_{yx}^{PHE}(\varphi) &= \Delta\sigma \sin\varphi \cos\varphi,
\end{aligned}
\tag{1}
$$

with $\Delta\sigma = \sigma_\parallel - \sigma_\perp$; $\sigma_\perp = \sigma_D$ the Drude conductivity, independent of the magnetic field ; $\sigma_\parallel = \sigma_D + a \times B^2$ with a a constant which depends on the carrier group velocities and the BC, and B the amplitude of the in-plane magnetic field ; and φ the relative angle between the magnetic and electric fields in the sample. As can be seen from Equation 1, the PHE is characterized by a π-periodic oscillation of both the longitudinal and transverse conductivities, when the magnetic field is rotated in-plane (while keeping the current direction fixed), with a $\pi/4$ offset between them, and the amplitude of the oscillations is expected to increase quadratically with magnetic field.

When the Weyl cones (WC) acquire a tilt (or an overtilt in the case of type-II Weyl cones), the field dependence of the PHE depends on the orientation of the current: when the current flows along the tilt direction, the amplitude of the PHE is expected to grow linearly for small magnetic fields. When the current flows perpendicular to the tilt direction however, the PHE is expected to grow quadratically with field, precisely as for non-tilted Weyl cones [3]. In real materials, the tilt vector can be pinned to principal crystallographic directions by multiple point-group symmetries (e.g. mirror symmetries). However, in materials with low-symmetry content the tilt vector will not be aligned with the crystallographic axes.

We note that, despite its historical name, the planar Hall effect is mostly a magnetism or band structure effect, and isn't typically linked to any Lorentz force from the (in-plane) magnetic field acting on the charge carriers.

Resistivity versus conductivity

We first recall that in magnetotransport experiments, we have no direct access to the conductivity. Instead, we measure the resistance of the sample, which is linked to the resistivity through the geometry of the sample. The behaviour of the resistivity contribution of the PHE is actually expected (in the type-I case at least) to follow very closely that of the conductivity [2, 6]:

$$
\begin{aligned}
\rho_{xx}^{PHE}(\varphi) &= \rho_\perp - \Delta\rho \, \cos^2\varphi, \\
\rho_{yx}^{PHE}(\varphi) &= -\Delta\rho \sin\varphi \cos\varphi,
\end{aligned}
\tag{2}
$$

with $\Delta\rho = \rho_\perp - \rho_\parallel$ the amplitude of the PHE ; $\rho_\perp = 1/\sigma_D$ constant in magnetic field ; and $\Delta\rho \propto B^2$ (in the type-I case). Note that the sign convention for $\Delta\rho$ from Ref. [2] is opposite that of $\Delta\sigma$ from Ref.[3].

While Equation 2 is the equation generally adopted in the community, we note that it is only valid in the absence of anisotropies in the zero-field conductivity matrix, i.e. when the Drude conductivity doesn't depend on the direction of the current ($\sigma_D(I_x) = \sigma_D(I_y)$). Even

in the absence of anisotropies, the quadratic field dependence of $\Delta\rho$ is only correct in the small oscillations limit, i.e. when $r = \Delta\sigma/\sigma_D << 1$. As this ratio increases (i.e. as the field increases), the field dependence of $\Delta\rho$ slows down, and it ultimately saturates at high field, with

$$\lim_{r\to\infty} \Delta\rho(r) = 1/\sigma_D.$$

Together with the mixed linear and quadratic field dependence terms expected in the case of tilted WCs, this may explain why most experimental papers studying the PHE in topological semi-metals have reported sub-quadratic field dependences [4, 16–18]. The expected angular dependence of the resistance is represented in Figure 2.a, with R_{xx} in blue and R_{yx} in red. The longitudinal resistance R_{xx} is maximal when magnetic field and current are aligned, while the transverse resistance R_{yx} vanishes in this configuration.

Planar Hall effect in nanostructures of t-PtBi$_2$

We studied the planar Hall effect in three exfoliated nanostructures of PtBi$_2$,contacted by standard e-beam lithography techniques. The samples used in this study are denoted as $D1$ (70 nm thick), $D2$ (126 nm thick) and $D4$ (41 nm thick), and their measurement configurations are shown in Figure 3. More details about the structures can be found in the methods section. In previous studies, the two-dimensional superconductivity of these samples was studied in details at sub-Kelvin temperatures [8], and an anomalous planar Hall effect was reported for $D1$ and $D2$ [12]. Here, we focus on measurements performed from room temperature down to 1 K, above the superconducting transition. No evidence of aging effects was observed between our studies, as indicated by the absence of any measurable change in the residual resistance ratio ($RRR = R(300K)/R(4K)$, see supplementary information Ref. [12]).

The PHE in PtBi$_2$ was measured first in 2-dimensional in-plane magnetic field mappings of the longitudinal and transverse resistance at 1 K with a 3D vector magnet (Figure 3). The resistance was measured using external lock-in amplifiers, with an AC current of 20 μA at a frequency of 113 Hz, with an integration time of 300 ms. Although the magnetic field range is limited to 1.5 T in either in-plane directions in this setup, the AMR and PHE are clearly visible in the mappings, through their π-periodicity and $\pi/4$ rotation between longitudinal and transverse measurements. The features at low field in Figure 3.g,h are associated with remnants of the superconductivity in the sample. We extract from the mappings the angular dependence of the resistance at fixed fields B_0, between 500 mT and 1.5 T. In order to have enough data points for analysis, we consider all points within 20 mT of B_0 (i.e. we extract all points with $|B - B_0| < 20$ mT).

The angular dependence obtained at 1.5 T and 1 K is shown for all three samples in Figure 3.j,k,l, and displays the features expected for the PHE for both longitudinal (R_{xx}, top panels) and transverse (R_{yx}, bottom panels) resistances. The maxima of longitudinal resistance correlate well with the expected orientation of the current in the samples. The data also shows some visible 2π-periodic signal, which may come from stray out-of-plane-field magnetoresistance (MR) due to a misalignment between the samples' planes and the magnetic field plane. We can fit the data very well using a constrained PHE model based on Equation 2, which takes into account a 2π-periodic contribution (more details on this model in the next sections, see Equation 4).

Field and temperature dependences of the PHE

To study the PHE in more details, we measured samples $D1$ and $D2$ in a Dynacool 14T PPMS using an insert equipped with a mechanical 2D rotator. By rotating the sample with the rotator, the angle φ between the fixed-axis magnetic field and the applied current can be adjusted over a full range of 360°. The resistance was measured using external lock-in amplifiers, with an AC current of 100 μA at a frequency of 927.7 Hz, with an integration time of 300 ms. In the main text, we will focus on results obtained for sample $D1$, although the same analysis was done for sample $D2$, with similar conclusions (see Supplementary Materials).

For measurements done at $T = 5$ K and $B = 1, 2, 3, 4, 5, 6, 7, 10$ T, as well as at $B = 14$ T and $T = 5, 10, 20, 50, 300$ K, 10 points were measured in succession at each angular position, and their resistance was averaged. The angular step for each measurement was 1°. More precise measurements were taken at $B = 14$ T and $T = 5, 100, 200$ K, with 40 points measured in succession at each angular position, and their resistance averaged. The angular step for each measurement was 0.5°, and the results were interpolated with a step of 1°, to perform the analysis in the same way for each pair of (B,T) parameters.

The measurements done at $T = 5$ K and $B = 14$ T are presented in Figure 4.a, and show a large π-periodic oscillation corresponding to the PHE. Again, the phase of the oscillations correlates well with the expected orientation of the current in the sample. The PHE is already visible at 1 T, the lowest magnetic fields measured (see Figure 5.a), and its magnitude increases with the magnetic field, with a power law that remains in very good agreements with the low field data (see Supplementary Materials). The amplitude of the PHE decreases with increasing temperature (Figure 5.b), and the PHE is very robust with temperature, and can be observed at 14 T up to room temperatures, as shown in Figure 4.c.

Analysis of the results

Beyond the π-periodicity and $\pi/4$ offset between the longitudinal and transverse oscillations, and the the correlation between the orientation of the current and the phase of the oscillations, an important characteristics of the PHE is the expected equal amplitude of both oscillations in resistivity (see Equation 2). A more complex analysis is required to confirm this point in real systems, as measurements can only access the resistance, and not the resistivity. In the ideal case, the conversion between the two follows the formulae:

$$R_{xx} = \frac{L}{W \times t} \cdot \rho_{xx} = \frac{N_\square}{t} \cdot \rho_{xx},$$
$$R_{yx} = \frac{1}{t} \cdot \rho_{yx}, \tag{3}$$

with L the distance between the longitudinal contacts, W the width of the sample, t its thickness, and $N_\square = L/W$ the number of squares between the longitudinal contacts. In this paper, and unless stated otherwise, we do not consider the thickness of the sample in this calculation (i.e. we take $t = 1$) as it doesn't change the relative amplitudes between R_{xx} and R_{yx}.

A careful analysis of the measurements is necessary, as we need to take into consideration the contributions of several additional signals, coming from different origins. First, as the shape of the samples deviates from the traditional Hall-bar, geometrically estimating accurately $N_\square$ between a pair of contacts is not trivial. This is further complicated by the position of the contacts on top of the flake, going inwards. It has been shown that such intrusive contacts can distort current flow and significantly reduce the measured amplitude of the transverse signal (possibly by as much as 50-75% in geometries similar to ours) [19]. We therefore consider an arbitrary reduction in the amplitude of the transverse resistance measured compared to its full amplitude.

Second, if the transverse contacts are not perfectly aligned orthogonally to the direction of the current, the resistance measured between them will include a longitudinal contribution, which can be significant as the longitudinal and transverse signals in the PHE have the same amplitude. In a traditional Hall configuration, such extra contributions due to contact misalignment can be removed by symmetrising (resp. asymmetrising) the longitudinal (resp. transverse) resistance in magnetic field, as the longitudinal and Hall signals are expected to be respectively even and odd in field. However in our system and configuration, such a procedure cannot be applied, such that we must consider an additional longitudinal contribution to the transverse resistance, with an arbitrary amplitude, in the fit.

Finally, as mentioned above, we must consider that the sample may not lie exactly in the rotation plane. When a magnetic field is applied in the rotation plane, this will result in a component of the magnetic field being perpendicular to the sample's plane, and thus in a regular magnetoresistance component in both longitudinal and transverse resistances. As the sample is rotated, the amplitude of the out-of-plane field will vary 2π-periodically, resulting in additional magnetoresistance contributions to the longitudinal and transverse resistances (with π- and 2π-periodicity, respectively). In order to account for any possible 2π-periodic background, we consider additional 2π-periodic signals in both resistances ($\mathrm{R}_{xx}^{2\pi}$ and $\mathrm{R}_{yx}^{2\pi}$). Any out-of-plane field component should therefore result in a deviation of the longitudinal resistance from our fit, as discussed in the next section.

When all these contributions are considered, our system can be described with

$$R_{xx}(B,\varphi) = \mathrm{R}_{xx}^{2\pi}(B,\varphi) + N_\square \cdot \rho_{xx}^{\mathrm{PHE}}(B,\varphi),$$
$$R_{yx}(B,\varphi) = \mathrm{R}_{yx}^{2\pi}(B,\varphi) + C_T \cdot \rho_{yx}^{\mathrm{PHE}}(B,\varphi) + C_L \cdot R_{xx}(B,\varphi), \tag{4}$$

with

$$\rho_{xx}^{\mathrm{PHE}}(\varphi) = \rho_\perp - \Delta\rho \cos^2 \varphi,$$
$$\rho_{yx}^{\mathrm{PHE}}(\varphi) = -\Delta\rho \cos\varphi \sin\varphi,$$
$$\mathrm{R}_{xx}^{2\pi}(B,\varphi) = A_{xx}(B)\cos(\varphi - \varphi_L),$$
$$\mathrm{R}_{yx}^{2\pi}(B,\varphi) = A_{yx}(B)\cos(\varphi - \varphi_T) + C. \tag{5}$$

Here, $\Delta\rho = \rho_\parallel - \rho_\perp$ is the amplitude of the PHE ; $\varphi = \widetilde{\varphi} - \varphi_{\mathrm{PHE}}$ is the angle between the magnetic field and the current in the sample, with $\widetilde{\varphi}$ the angular position of the sample set by the rotator and φ_{PHE} the rotator angle for which current and field are aligned ; $\mathrm{R}_{xx}^{2\pi}$ and $\mathrm{R}_{yx}^{2\pi}$ are 2π-periodic background contributions with arbitrary angular origins φ_L and φ_T ; C is a field-independent offset of the transverse resistance ; and $N_\square$, C_T and C_L are respectively the effective number of squares between longitudinal contacts, the correcting factor for the transverse resistance due to the invasive contacts, and the correcting factor due to the misalignment of the contacts. The same analysis is performed in temperature, with the addition of a temperature-dependent vertical offset to the background terms to account for the resistance increasing with temperature:

$$\mathrm{R}_{xx}^{2\pi}(T,\varphi) = A_{xx}(T)\cos(\varphi - \varphi_L) + C_{xx}(T),$$
$$\mathrm{R}_{yx}^{2\pi}(T,\varphi) = A_{yx}(T)\cos(\varphi - \varphi_T) + C_{yx}(T). \tag{6}$$

Due to the large number of unknown parameters, it is not possible to get meaningful values for the different variables by fitting a single set of angular dependence (i.e. $R_{xx}(B_0,\varphi)$ and $R_{yx}(B_0,\varphi)$) with Equation 4. We can however overcome this issue by noting that most of these parameters are geometric and therefore independent of the external magnetic field. Thus, by fitting $R_{xx}(B,\varphi)$ and $R_{yx}(B,\varphi)$ together at multiple fields B, and fixing

the geometric parameters as global parameters across all fits, we can extract meaningful values for each parameter, and recover the amplitude of the PHE in resistivity.

The results obtained are shown as thick lines in Figure 4, and present an excellent agreement with the experimental data for both samples, with only small deviations from the model at low fields and high temperatures, which we will discuss shortly (see Figure 6). The dependence of the PHE amplitude $\Delta\rho$ with field and temperature is shown in Figure 5. $\Delta\rho$ increases with field, following the power laws $\Delta\rho \propto B^{1.24}$, which is consistent with low field measurements (see Supplementary materials), and is notably lower than the expected quadratic behavior expected for the pure chiral anomaly effect [2].

As mentioned before, both BC effects and orbital magnetic moment effects could contribute to this sub-quadratic field dependence [20]. Importantly, $\Delta\rho$ starts decreasing with temperature above $T \sim 20$ K, and remains clearly visible up to room temperature, with $\Delta\rho \simeq 0.34$ $\mu\Omega$.cm, which is relatively large for a non-magnetic system.

DEVIATIONS FROM PHE MODEL

As stated above, and as can be seen in Figure 4.c, the constrained model of Equation 4 deviates from the data towards low magnetic fields and high temperatures. In the following, we will detail and analyse these deviations and provide possible explanations.

Planar Hall effect at low field and at high temperature

At low temperature $T = 5$ K and low magnetic fields $B \leq 3$ T, while the oscillations from the PHE are still clearly visible in both samples (see Figure 6.a,b,c), the constrained model (thick lines) deviates significantly from the data, due mainly to an phase offset of the oscillations as well as a vertical offset. The amplitude of the oscillations is however well represented by the model. Both offsets decrease quickly with field. At high field ($B = 14$ T) and high temperature $T \geq 100$ K on the other hand, there are no vertical or phase offsets between the constrained model and the data. However, while the model still fits closely the data in R_{yx}, it starts deviating at high temperatures from the data in R_{xx}, as shown in Figure 6.e,f,g (thick lines). This is due to both oscillations no longer sharing the same amplitude, which is incompatible with the PHE model. In order for the fit to keep converging meaningfully at high temperature, we chose to artificially give a higher weight to the data in R_{yx} than in R_{xx}, which is why the deviations is seen only in R_{xx}.

Simple model

While the data deviates from the constrained model of Equation 4, we note that the general shape of the data can still accurately be described by π-periodic oscillations. Thus, to study the deviations from the constrained model in more details, we fitted the data for R_{xx} and R_{yx} independently with an unconstrained model, which includes only two contributions: π-periodic, and 2π-periodic:

$$R(\varphi) = C + A^{2\pi} \cdot \cos\left(\varphi - \varphi_{2\pi}\right) + A^{\pi} \cdot \cos\left[2(\varphi - \varphi_{\pi})\right], \tag{7}$$

with C an angle-independent constant, and A^{π} and $A^{2\pi}$ the amplitudes of the π- and 2π-periodic signals, with angular origins φ_{π} and $\varphi_{2\pi}$, respectively. The results are shown in Figure 6 in dashed lines, and fit the data closely at all fields and temperatures.

The phase and amplitude of the π-periodic oscillations in R_{xx} and R_{yx} can be extracted from this model, and the field and temperature dependence are shown in Figure 6.d,h. For comparison, we show the amplitudes reduced by their values at $B = 14$ T, $T = 5$ K. We also subtract 45° from the phase in R_{yx}, to account for the expected $\pi/4$ shift between R_{yx} and R_{xx}. As expected, the amplitudes of the oscillations in R_{xx} and R_{yx} have the same field dependence at low temperature, in both samples (see Figure 6.d, top panel). The phase of the oscillations, however, shows a strong variation at low magnetic field (Figure 6.d, bottom panel). While the phase of the oscillations in R_{yx} stabilizes quickly, at about 2 T, it continues increasing slowly in R_{xx} over the full angular range. The difference in phase for both oscillations eventually come within a few degrees of the expected $\pi/4$ at higher field, without reaching that value. The other sample, $D2$, shows slightly different features (see Supplementary materials), with only a small variability of the phase at low field, which might be attributed to a lower signal-to-noise ratio. The shift between the oscillations in R_{xx} and R_{yx} deviates from the expected value of 45° by about 5°, which remains about constant over the entire magnetic field range. The variability of the phase in $D1$ might be related to current jetting in the sample, which does not have a standard Hall bar shape: If the current lines change orientation as the magnetic field is increased, e.g. to minimize the magnetoresistance, this could lead to a change in the phase of the PHE, which depends on the relative orientation of the magnetic field and the current. As $D2$ is closer to the Hall bar shape, the effect of current jetting would be expected to be lower, and the phase variation in field attenuated as well. The deviation from the $\pi/4$ offset between R_{xx} and R_{yx} might also be related to the shape of the samples: As neither $D1$ nor $D2$ are perfect Hall bars, the resistance between the transverse contacts will also include a longitudinal

contribution. Since $a \cdot \cos\phi + b \cdot \sin\phi = R \cdot \cos(\phi - \alpha)$, with $R = \sqrt{a^2 + b^2}$ and $\alpha = \tan^{-1}(b/a)$, the longitudinal contribution is equivalent to a renormalization and phase offsetting of the transverse signal.

The same analysis is performed at $B = 14$ T and temperatures ranging from $T = 5$ K to $T = 300$ K, and the results are shown in Figure 6.h. As expected, no large variation is observed in the phase of the oscillations, with a few degrees separating the phase in R_{xx} and R_{yx}, as before. However, the temperature dependence of the amplitude of the oscillations is now different between the two resistances, with the amplitude in R_{xx} decreasing more slowly than in R_{yx}. This effect is clearly visible in both samples (see Supplementary materials for D2), and is the reason for the deviation between the constrained model and the data.

There are, broadly, two mechanisms which could cause this discrepancy between R_{xx} and R_{yx}. The first mechanism relates to the geometry of the sample and the flow of current. In our analysis, we have considered these parameters (i.e. $N_\square, C_T, C_L$ etc.) as independent of magnetic field and temperature. As these parameters relate the resistance to the resistivity, they provide us directly with the link between the amplitude of the oscillations between R_{xx} and R_{yx}. However, if (some of) these parameters were to vary with temperature, this would change the expected balance between the two amplitudes, and may cause the observed discrepancy. Although the exact geometry of the current flow may vary slightly with temperature due to inhomogeneities in the sample, for instance around the invasive contacts, leading to slightly different temperature dependence of the resistance, we cannot think of an effect strong enough to cause the observed difference in amplitude. The second mechanism would be the existence of a second π-periodic effect in R_{xx}, distinct from the PHE. This effect would need to have a small amplitude at low temperature with respect to the PHE, as the latter accounts well for the data at low temperature. If such an effect did exist, and its amplitude decreased more slowly than that of the PHE, then the balance between this effect and the PHE would change as the temperature increases, with the PHE becoming less predominant at higher temperature, leading to the extra signal observed. One possibility for such a signal would be a contribution to the magnetoresistance from a small out-of-plane magnetic field $B_\perp$, due to a misalignment between the sample's plane and the rotation plane of the rotator. Such a misalignment would result in a 2π-periodic variation of $B_\perp$ around $B_\perp = 0$, as the sample is rotated. This would result in a 2π-periodic contribution to R_{yx}, as the Hall resistance is odd in out-of-plane field, but would give a π-periodic contribution in R_{xx}, as the longitudinal resistance is even in out-of-plane field. A tilt of the sample with respect to the rotation plane would therefore result in an additional π-periodic contribution in R_{xx}, with no such additional contribution in

R_{xx}. Depending on the axis of this tilt with respect to the orientation of the current in the sample, this additional contribution would either add up to or cancel out some of the oscillation due to the PHE. We note that a misalignment of the rotation plane with respect to the magnetic field axis would result in a constant out-of-plane field, independent on the angular position of the sample, and would therefore not have an influence on the π-periodic signal. As the PHE and the longitudinal magnetoresistance (LMR) are not expected to fully share a common physical origin in our material , they have no reason to share a similar temperature dependence. It is therefore possible that the LMR has a slower decrease in temperature than the PHE, and could account for the additional oscillation seen in our measurements.

DISCUSSION

The band structure of t-PtBi$_2$ is quite complex from a topological perspective. As we reported previously, DFT calculations show that t-PtBi$_2$ is a Weyl semi-metal with 12 symmetry-related Weyl nodes (see Figure 1) close to the the Fermi energy [8] (~ 45 meV above E_F). This prediction was later experimentally confirmed by ARPES [10] and STM [11] experiments, in which the Fermi arcs (topological surface states associated with the Weyl nodes) where observed, although no transport signature of the topology of t-PtBi$_2$ nanostructures (aside from the anomalous planar Hall effect [12] has been reported as of now. Since then, more detailed calculations [12] have found the existence of 3 additional groups of 12 (each) symmetry-related Weyl nodes at higher energies, at ~ 141 meV, ~ 300 meV and ~ 320 meV above E_F respectively , as well as topological nodal lines - 1D continuous band touchings - in the band structure between the HOMO and LUMO bands (see [12], and SM). While assigning a quantitative weight to the contributions of each such topological features to the observed PHE is far beyond the scope of this study, the contribution from the group of 12 Weyl nodes closest to the Fermi energy is likely to dominate (see more detailed discussion in SM).

The most well known transport signature of topological semi-metals is the negative longitudinal magnetoresistance, which is associated with the chiral anomaly [21]. However, it has been recently understood that in Weyl semi-metals effects of orbital magnetic moments could result both in a positive longitudinal magnetoresistance [22] and in a positive transversal magnetoresistance [20] when considering tilted Weyl cones. The anisotropy in these responses is expected to lead to a PHE that therefore represents one of the main transport signature in topological semi-metals. It is important to point out that the observation of a PHE in non-magnetic mate-

rials does not necessarily imply the presence of topological degeneracies. The Lorentz-force induced orbital magnetoresistance [23] is also expected to be anisotropic due to cancellation of Lorentz force with collinear electric and magnetic fields and can therefore yield a PHE. In this regard, it is important to note that a very large magnetoresistance (with out-of-plane magnetic field) has been reported in $PtBi_2$ [8]. We can thus expect the orbital magnetoresistance to be significant, and therefore its anisotropies could contribute to a PHE.

Nonetheless, our measurements are consistent with the predictions of Weyl physics in $PtBi_2$, and furthermore all our results can be understood in that context, without needing to invoke additional effects. The observation of a PHE in $PtBi_2$ therefore reinforces with charge-transport previous observations from spectroscopy techniques [10, 11] as to its Weyl nature.

CONCLUSION

In this paper, we presented the first measurement of the planar Hall effect in nanostructure of the van-der-Waals layered non-magnetic type-I Weyl semi-metal trigonal-$PtBi_2$, and study their dependence in magnetic field and temperature. The discovery of a PHE in $PtBi_2$ is significant, as it is an expected signature of Weyl semi-metals. We have found that the PHE is present already at magnetic fields as low as 1 T, and is robust up to room temperature. We also unveiled some deviations from the theoretical expectations for the PHE in Weyl semi-metals, with a sub-quadratic field dependence of the amplitude, which may originate from a combination of the Weyl-cones' tilt (e.g. from some type-II Weyl nodes originating from the nodal lines) and a deviation from the simple sine-wave model when the amplitude of the oscillations is large.

Overall, this study reinforces our understanding of the quantum geometry of trigonal-$PtBi_2$, which is of particular interest in the context of the recent discovery of superconductivity in this material, with two-dimensional superconductivity reported in bulk nanostructures, and surface Fermi-arc supported superconductivity seen in ARPES.

METHODS AND SM

Methods

Sample Preparation

The high-quality single crystals of $PtBi_2$ were synthesized using the self-flux technique, as described in [24]. The single crystals we measured could reach Residual Resistance Ratios (RRR) up to $RRR \sim 130$, as shown in

[8] (in SM). Thin flakes, with widths exceeding 10 μm and thicknesses ranging from a few dozen to several hundred nanometers, were obtained via mechanical exfoliation. Electrical contacts were fabricated using Cr/Au deposition through standard e-beam lithography methods. To remove surface oxidation before metal deposition, a light Ar etching process was performed by IBE.

The primary sample examined in this study, labeled $D1$, has a thickness of 70 nm. Additional data includes complementary results from a second sample, $D2$ (126 nm thick). A third sample, $D4$ (41 nm), was measured at low temperatures in a vector magnet (see Figure 3) but was unfortunately damaged before further measurements could be conducted.

No indications of aging effects were observed between the two experimental sessions, as confirmed in $D1$ by the stability of the residual resistance ratio ($RRR = R(300K)/R(4K)$), which remained unchanged (see [12], SM). The RRR of the different samples, as reported in [8], was 8.7 for $D1$ (70nm), 13.6 for $D2$ (126nm) and 4.7 for $D4$ (41nm).

Measurement Setup

The sample is arranged in a conventional Hall-bar geometry. A current is applied between the source and drain, as illustrated in Figure 3.a,b,c.

Longitudinal and transverse resistances, shown in blue and red respectively, are measured along and perpendicular to the sample with respect to the current direction.

Vector magnet measurements

The PHE in t-$PtBi_2$ was measured first in 2-dimensional in-plane magnetic field mappings of the longitudinal and transverse resistance at 1 K with a 3D vector magnet (Figure 3). The resistance was measured using external lock-in amplifiers, with an AC current of 20 μA at a frequency of 113 Hz, with an integration time of 300 ms.

To extract the angular dependence of the resistance from the mappings (at a fixed field B_0 between 500 mT and 1.5 T), we considered all points within the annulus centered around $B_0 : |B - B_0| < 20$ mT. These points were then ordered by their angle φ, and the resulting list was interpolated to a uniform 1° step. The width of the annulus was selected to be large enough to include enough points (over the full angular range) for the analysis to be meaningful, while being small enough to avoid the data at "fixed field" being over-influenced by the field dependence of the PHE.

Variable temperature insert measurements

Additional measurements were performed using a Dynacool 14T PPMS, in a mechanical 2D rotator-equipped insert.

By changing the sample's orientation with the rotator, the angle φ between the applied current and the fixed-axis magnetic field could be varied continuously over a full 360° range, where φ represents the angle between the magnetic and electric fields.

Resistances were measured with external lock-in amplifiers, by injecting an AC current of 100 μA at a frequency of 927.7 Hz, and an integration time of 300 ms. At these low currents, thermal effects are negligible. For sample $D1$, measurements were taken at $T = 5$ K for magnetic fields of $B = 1, 2, 3, 4, 5, 6, 7, 10$ T, and at $B = 14$ T for temperatures $T = 5, 10, 20, 50, 300$ K. At each angular position, the resistance was measured 10 times and then averaged. An angular step of 1° was used for these measurements. Identical measurement conditions were applied to sample $D2$.

For sample $D1$, higher-precision measurements were carried out at $T = 5$ K and $B = 14$ T, as well as at $B = 14$ T for $T = 100, 200$ K. These measurements involved averaging over 40 points at each angular position, with a 0.5° angular step. The data were then interpolated to a 1° step to ensure uniform analysis across all (B,T) measurements.

A high-frequency noise component appears superimposed on the π-periodic oscillation for both $D1$ and $D2$, with a stronger presence in the latter. This noise likely originates from the mechanical rotator: when the stepper motor at the top of the measurement stick rotates by a small angle (e.g., 1°), the corresponding movement of the rotator inside the cryostat is not perfectly uniform, fluctuating around the intended step size.

Since the rotator's angle is measured at the top of the stick (rather than the sample's exact position at the bottom), these discrepancies introduce minor deviations in the planar Hall effect (PHE) signal from an ideal π-periodic oscillation. These artifacts are reproducible and diminish with increasing temperature, which is consistent with expected mechanical inaccuracies in the rotator.
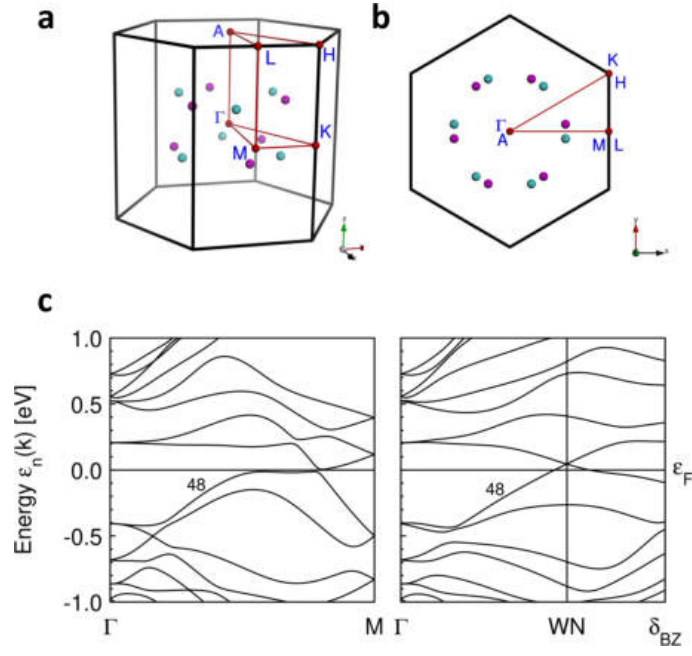
FIG. 1. **a,b**: Brillouin zone showing the 12 symmetry-related Weyl nodes in band 48 (see [12] closest to the Fermi level, with colour-encoded chirality. **c**: Band structure along the ΓM line (left panel) and from Γ to the Brillouin zone boundary through the blue Weyl node closest to the ΓM line.
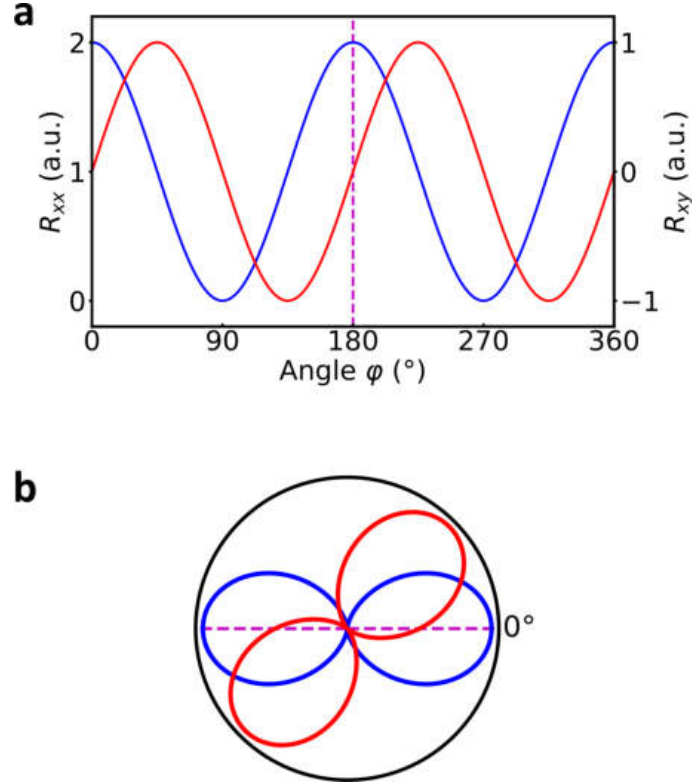
FIG. 2. **a,b**: Typical angular dependence of the conventional planar Hall effect, in Cartesian (**a**) and polar (**b**) coordinates. Both the longitudinal (anisotropic magnetoresistance, R_{xx}, blue) and transverse (planar Hall effect, R_{yx}, red) resistances exhibit a π-periodic angular dependence, with a $\pi/4$-offset between them. The origin of the oscillation is set by the direction of the electric field (current).
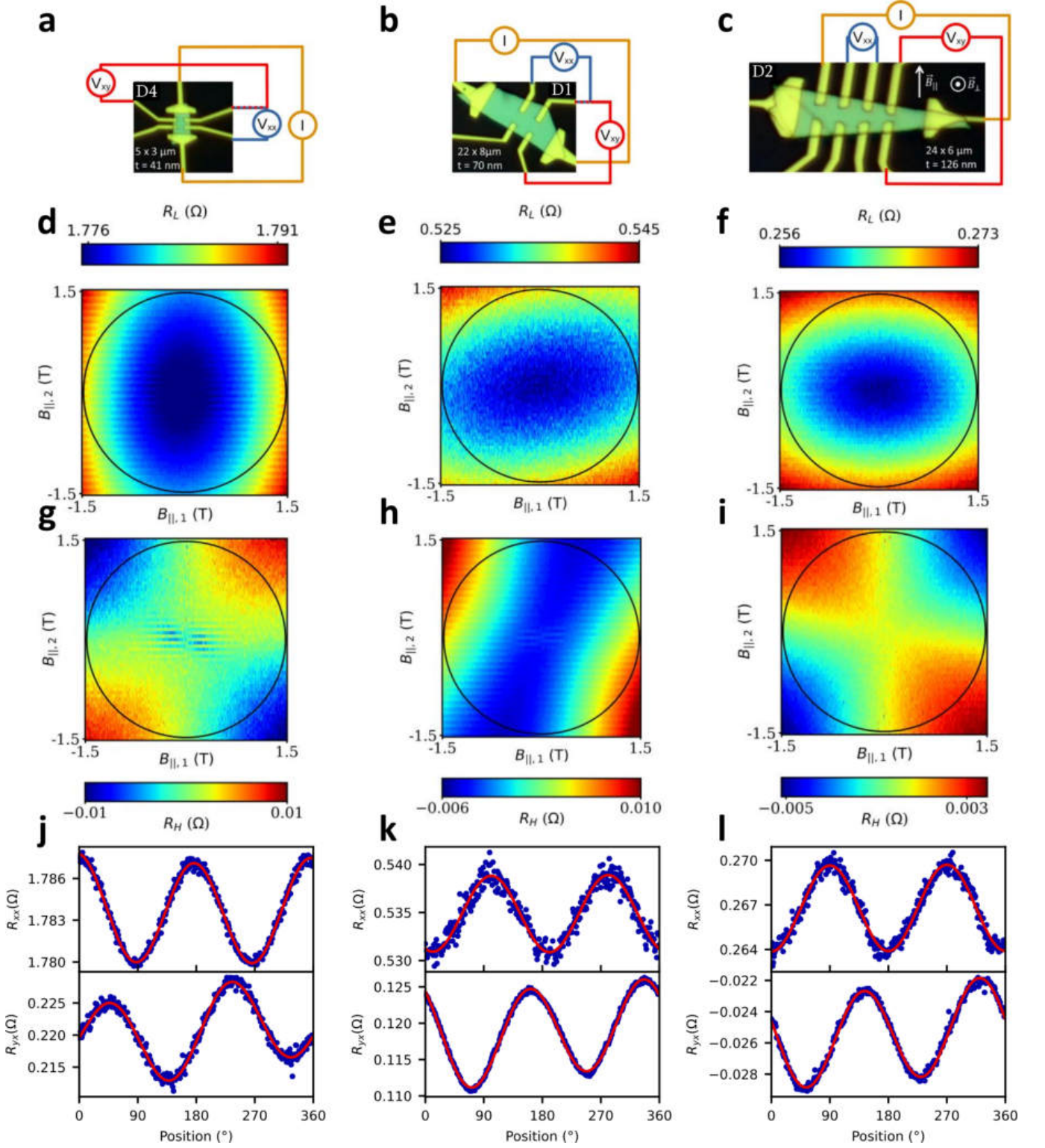
FIG. 3. **a,b,c**: Optical pictures and sample configurations for D4 (41 nm), D1 (70 nm) and D2 (126 nm). The measurements related to each sample is shown below it. **d-i**: In-plane magnetic field $(B_y - B_z)$ mappings of the longitudinal $(R_{xx}$, d,e,f) and transverse $(R_{yx}$, g,h,i) resistances. All mappings were measured simultaneously by sweeping $B_{\parallel,1}$) at fixed $B_{\parallel,2}$, and increasing $B_{\parallel,2}$ in steps of 50 mT. All mappings show the expected four-fold symmetry expected for the PHE, with sample-orientation-dependent phase and $\pi/4$ shift between longitudinal and transverse configurations. **j-l**: Angular dependence of R_{xx} (top panels) and R_{yx} (bottom panels) extracted from the mappings **d-i**, for a field $B = 1.5$ T corresponding to the black circles. The data is well fitted by the PHE model (in red, see Equation 4). The phase of the oscillations in each sample can be correlated to the presumed current orientation in the sample.
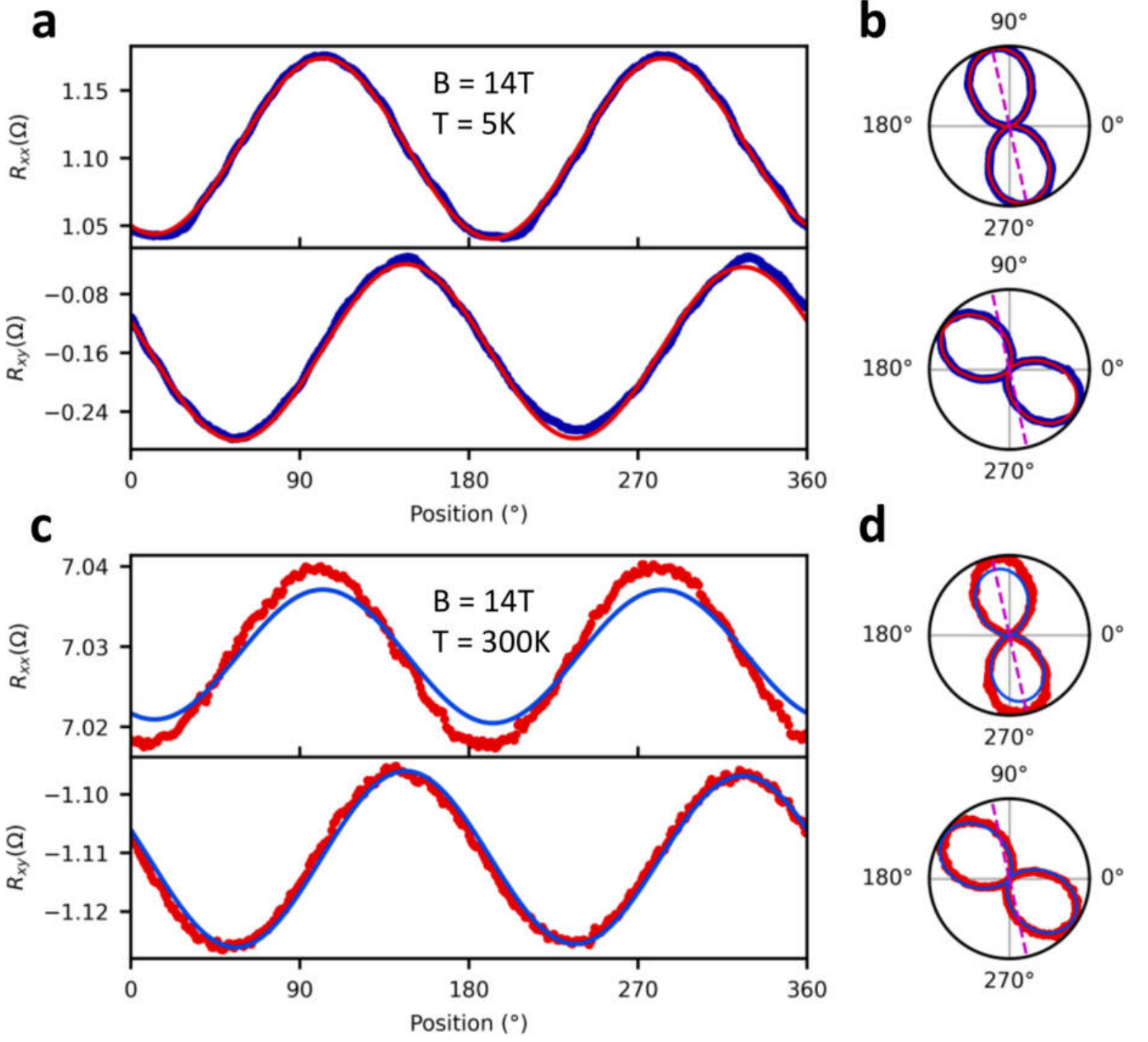
FIG. 4. **a,c**: Angular dependence at 14 T and 5 K (a) or 300 K (c) of the longitudinal (R_{xx}, top panels) and transverse (R_{yx}, bottom panels) resistances for sample D1, in Cartesian coordinates. Fits to the PHE model (Equation 4 are shown in red (a) and blue (c). **b,d**: Same data as in **a,c**, in polar coordinates. The dashed-line represents the orientation of the current estimated from the data. [a]

[a] We note that, although the raw data shown is the same as in [12], the fits in the present figure are different from that other study, as the latter were unconstrained π- and 2π-periodic signals, while the presents ones are heavily constrained, as discussed in the main text.
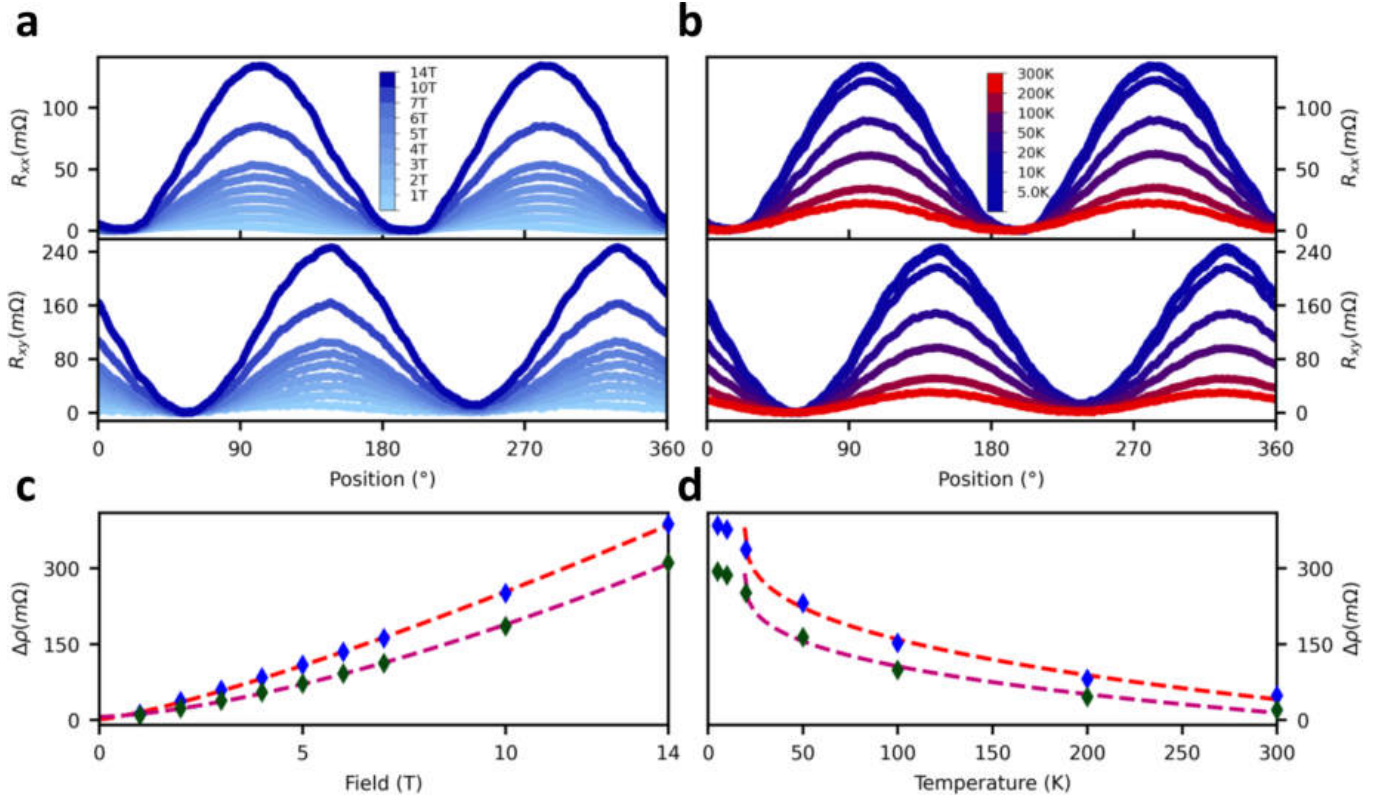
FIG. 5. **a,b**: Angular dependence of the longitudinal (R_{xx}, top panels) and transverse (R_{yx}, bottom panels) resistances of samples D1 at 5K and multiple fields from 1T to 14T (a) and at 14T and multiple temperatures from 5K to 300K (b). The plots are shifted vertically for visibility, to share a minimum at 0 Ω. **c,d**: Field (c) and temperature (d) dependence of the PHE amplitude $\Delta\rho$ extracted from fits of the data in (a,b) with Equation 4 for samples D1 (blue diamonds and dashed-red line, respectively), and for sample D2 (green diamonds and dashed-magenta line, respectively, see SM). The field dependence of $\Delta\rho$ is well fitted with a sub-quadratic power law for both samples. The temperature dependence of $\Delta\rho$ cannot be fitted with an exponential decay law, and is fitted with a power law.
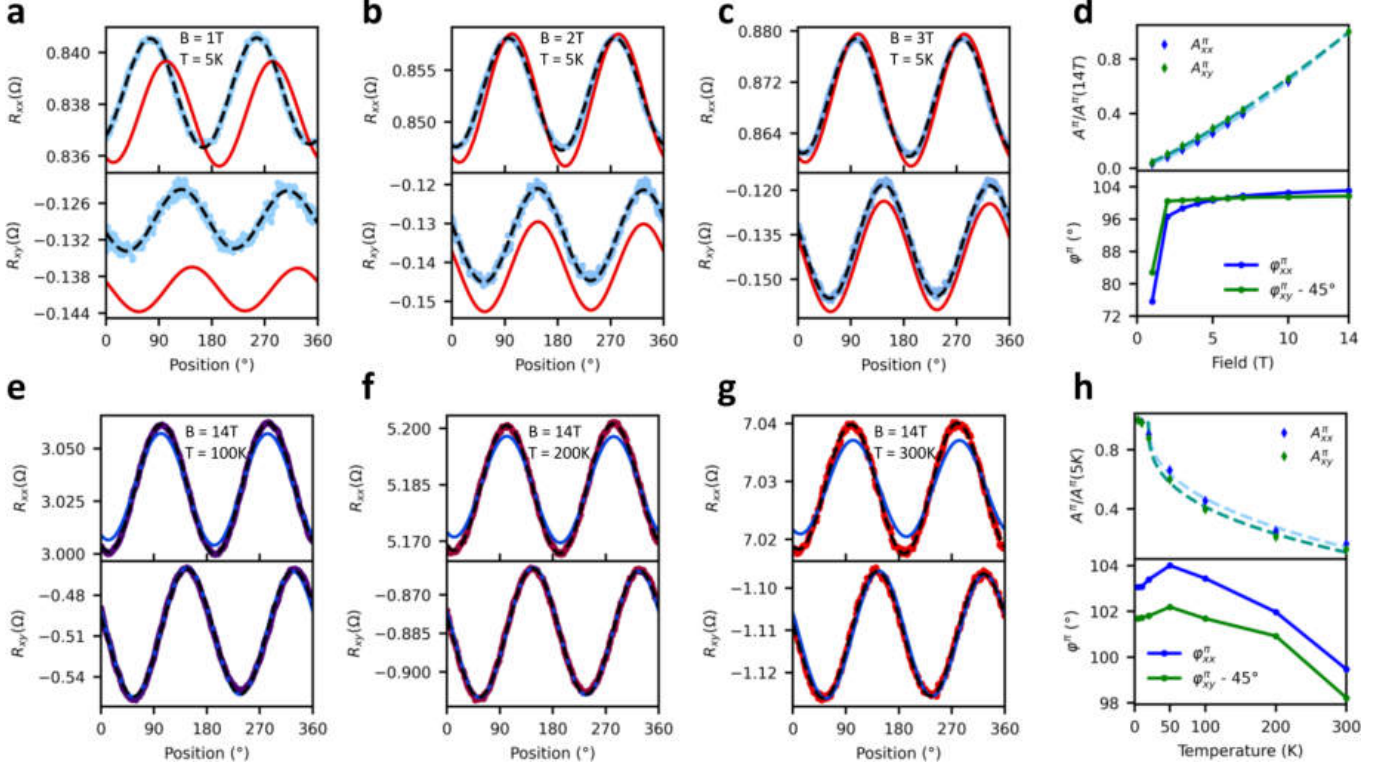
FIG. 6. **a,b,c**: Angular dependence of the longitudinal (R_{xx}, top panels) and transverse (R_{yx}, bottom panels) resistances at 5 K and 1T (a), 2T (b) and 3T (c). As the result of dephasing and unaccounted-for offset, the constrained fits of the PHE model (Equation 4, in red) start deviating from the measurements at low fields. The data can still be fitted very well with an unconstrained π-periodic fit (in dashed black). **d**: Field dependence of the amplitude (top panel, renormalized to its value at 14T) and phase (bottom panel) of the unconstrained fits of the longitudinal (R_{xx}, blue) and transverse (R_{yx}, green) resistances. The renormalized amplitudes of the oscillations in R_{xx} and R_{yx} have the same field dependence, as expected for the PHE, however the phase of the oscillations can change significantly with the magnetic field. **e,f,g**: Angular dependence of the longitudinal (R_{xx}, top panels) and transverse (R_{yx}, bottom panels) resistances at 14 T and 100 K (e), 200 K (f) and 300 K (g). The constrained fits of the PHE model (Equation 4, in blue) start deviating from the measurements in R_{xx} at high temperature, as the amplitude of the oscillations are smaller than anticipated from those in R_{yx}. The data can still be fitted very well with an unconstrained π-periodic fit (in dashed black). **h**: Temperature dependence of the amplitude (top panel, renormalized to its value at 5 K) and phase (bottom panel) of the unconstrained fits of the longitudinal (R_{xx}, blue) and transverse (R_{yx}, green) resistances. The renormalized amplitudes of the oscillations in R_{xx} and R_{yx} have a different dependence in temperature, as the amplitude in R_{xx} decreases more slowly than that in R_{yx}. The phase of the oscillations changes slightly with the temperature.

* arthur.veyrat@universite-paris-saclay.fr
† cortix@unisa.it
‡ j.dufouleur@ifw-dresden.de

[1] X. Wan, A. M. Turner, A. Vishwanath, and S. Y. Savrasov, Physical Review B - Condensed Matter and Materials Physics **83**, 1 (2011).

[2] A. A. Burkov, Physical Review B **96**, 041110 (2017).

[3] S. Nandy, G. Sharma, A. Taraphder, and S. Tewari, Physical Review Letters **119**, 1 (2017).

[4] N. Kumar, S. N. Guin, C. Felser, and C. Shekhar, Physical Review B **98**, 1 (2018), arXiv:1711.04133.

[5] R. Singha, S. Roy, A. Pariari, B. Satpati, and P. Mandal, Physical Review B **98**, 081103 (2018), arXiv:1806.08287.

[6] Q. Liu, F. Fei, B. Chen, X. Bo, B. Wei, S. Zhang, M. Zhang, F. Xie, M. Naveed, X. Wan, F. Song, and B. Wang, Phys. Rev. B **99**, 155119 (2019).

[7] A. A. Taskin, A. A. Taskin, A. A. Taskin, H. F. Legg, F. Yang, S. Sasaki, S. Sasaki, Y. Kanai, K. Matsumoto, A. Rosch, and Y. Ando, Nature Communications **8**, 1340 (2017).

[8] A. Veyrat, V. Labracherie, D. L. Bashlakov, F. Caglieris, J. I. Facio, G. Shipunov, T. Charvin, R. Acharya, Y. Naidyuk, R. Giraud, J. van den Brink, B. Büchner, C. Hess, S. Aswartham, and J. Dufouleur, Nano Lett. 10.1021/acs.nanolett.2c04297 (2023).

[9] S. Schimmel, Y. Fasano, S. Hoffmann, J. Puig, G. Shipunov, D. Baumann, S. Aswartham, B. Büchner, and C. Hess, High-TC surface superconductivity in topological Weyl semimetal t-PtBi2 (2023), arXiv:2302.08968 [cond-mat].

[10] A. Kuibarov, O. Suvorov, R. Vocaturo, A. Fedorov, R. Lou, L. Merkwitz, V. Voroshnin, J. I. Facio, K. Koepernik, A. Yaresko, G. Shipunov, S. Aswartham, J. V. D. Brink, B. Büchner, and S. Borisenko, Nature **626**, 294 (2024).

[11] S. Hoffmann, S. Schimmel, R. Vocaturo, J. Puig, G. Shipunov, O. Janson, S. Aswartham, D. Baumann, B. Büchner, J. van den Brink, Y. Fasano, J. I. Facio, and C. Hess, Fermi arcs dominating the electronic surface properties of trigonal PtBi$_2$ (2024), arXiv:2407.15790 [cond-mat].

[12] A. Veyrat, K. Koepernik, L. Veyrat, G. Shipunov, I. Kovalchuk, S. Aswartham, J. Qu, A. Kumar, M. Ceccardi, F. Caglieris, N. Pérez, R. Giraud, B. Büchner, J. van den Brink, C. Ortix, and J. Dufouleur, Nature Communications **16**, 6711 (2025).

[13] W. Thomson, Proc. R. Soc. Lond. **8**, 546 (1857).

[14] K. Hong and N. Giordano, Phys. Rev. B **51**, 9855 (1995).

[15] A. A. Burkov, Journal of Physics Condensed Matter **27**, 10.1088/0953-8984/27/11/113201 (2015), arXiv:1502.07609.

[16] P. Li, C. Zhang, Y. Wen, L. Cheng, G. Nichols, D. G. Cory, G.-X. Miao, and X.-X. Zhang, Physical Review B **100**, 205128 (2019).

[17] D. D. Liang, Y. J. Wang, W. L. Zhen, J. Yang, S. R. Weng, X. Yan, Y. Y. Han, W. Tong, W. K. Zhu, L. Pi, and C. J. Zhang, AIP Advances **9**, 055015 (2019).

[18] J. Meng, H. Xue, M. Liu, W. Jiang, Z. Zhang, J. Ling, L. He, R. Dou, C. Xiong, and J. Nie, J. Phys.: Condens. Matter **32**, 015702 (2019).

[19] J. G. Gluschke, J. Seidl, H. H. Tan, C. Jagadish, P. Caroff, and A. P. Micolich, Nanoscale **12**, 20317 (2020).

[20] K. Das and A. Agarwal, Phys. Rev. B **100**, 085406 (2019), arXiv:1903.01205 [cond-mat.mes-hall].

[21] D. T. Son and B. Z. Spivak, Physical Review B - Condensed Matter and Materials Physics **88**, 1 (2013), arXiv:1206.1627.

[22] A. Knoll, C. Timm, and T. Meng, Phys. Rev. B **101**, 201402 (2020), arXiv:1912.07852 [cond-mat.mes-hall].

[23] Y. Cui, Z. Li, H. Chen, Y. Wu, Y. Chen, K. Pei, T. Wu, N. Xie, R. Che, X. Qiu, Y. Liu, Z. Yuan, and Y. Wu, Science Bulletin **69**, 2362 (2024).

[24] G. Shipunov, I. Kovalchuk, B. R. Piening, V. Labracherie, A. Veyrat, D. Wolf, A. Lubk, S. Subakti, R. Giraud, J. Dufouleur, S. Shokri, F. Caglieris, C. Hess, D. V. Efremov, B. Büchner, and S. Aswartham, Physical Review Materials **4**, 124202 (2020), arXiv:2002.03976.

Planar Hall effect in nanostructures of trigonal-PtBi₂: Supplementary Materials

Arthur Veyrat,[1, 2, 3, *] Klaus Koepernik,[1, 2] Louis Veyrat,[1, 2, 4] Grigory Shipunov,[1, 2]
Iryna Kovalchuk,[5, 1] Saicharan Aswartham,[1, 2] Jiang Qu,[1, 2] Ankit Kumar,[1, 2] Michele
Ceccardi,[6, 7] Federico Caglieris,[7] Nicolás Pérez Rodríguez,[1, 2] Romain Giraud,[1, 2, 8] Bernd
Büchner,[1, 2, 9] Jeroen van den Brink,[1, 2, 9] Carmine Ortix,[10, †] and Joseph Dufouleur[1, 2, 11, ‡]

[1] *Leibniz Institute for Solid State and Materials Research (IFW Dresden), Helmholtzstraße 20, D-01069 Dresden, Germany*
[2] *Würzburg-Dresden Cluster of Excellence ct.qmat, Dresden, Germany*
[3] *Laboratoire de Physique des Solides (LPS Orsay), 510 Rue André Rivière, 91400 Orsay, France*
[4] *CNRS, Laboratoire National des Champs Magnétiques Intenses, Université Grenoble-Alpes,*
Université Toulouse 3, INSA-Toulouse, EMFL, 31400 Toulouse, France
[5] *Kyiv Academic University, 03142 Kyiv, Ukraine*
[6] *Department of Physics, University of Genoa, 16146 Genoa, Italy*
[7] *CNR-SPIN Institute, 16152 Genoa, Italy*
[8] *Université Grenoble Alpes, CNRS, CEA, Grenoble-INP, Spintec, F-38000 Grenoble, France*
[9] *Department of Physics, TU Dresden, D-01062 Dresden, Germany*
[10] *Dipartimento di Fisica "E. R. Caianiello", Universitá di Salerno, IT-84084 Fisciano (SA), Italy*
[11] *Center for Transport and Devices, TU Dresden, D-01069 Dresden, Germany*

SUPPLEMENTARY MATERIALS

Resistivity in the planar Hall effect

It is expected from the theory [1] that the planar Hall effect (PHE) component of the conductivity follows the angular dependence

$$
\begin{aligned}
\sigma_{xx}^{\text{PHE}}(\varphi) &= \sigma_\perp + \Delta\sigma \cos^2\varphi, \\
\sigma_{yx}^{\text{PHE}}(\varphi) &= \Delta\sigma \cos\varphi \sin\varphi,
\end{aligned}
\tag{1}
$$

with $\Delta\sigma = \sigma_\parallel - \sigma_\perp$ the amplitude of the oscillation, $\sigma_\perp$ and $\sigma_\parallel$ the conductivity when the in-plane magnetic field is orthogonal or parallel to the electric field (i.e. the current), and φ the angle between the magnetic field and the current. When the PHE originates from the chiral anomaly in Weyl semimetals, it is expected that $\sigma_\perp$ is constant in magnetic field, with $\sigma_\perp = \sigma_D$ the drude conductivity, and $\sigma_\parallel = \sigma_D + a \cdot B^2$ increases with magnetic field. In order to obtain the resistivity matrix, we must inverse the conductivity matrix $\sigma = \begin{pmatrix} \sigma_{xx} & \sigma_{xy} \\ \sigma_{yx} & \sigma_{yy} \end{pmatrix}$. From Onsager relations, we have $\sigma_{yx}(B) = \sigma_{xy}(-B)$. Since the magnetic field is in the plane, $\sigma_{xy}(-B, \varphi) = \sigma_{xy}(B, \varphi + \pi) = \sigma_{xy}(B, \varphi)$ as σ_{xy} is π-periodic. Hence, we have $\sigma_{yx}(B) = \sigma_{xy}(B)$. We can also note that σ_{yy} can be expressed similarly to σ_{xx} by simply exchanging $\sigma_\parallel$ and $\sigma_\perp$: $\sigma_{yy}(\varphi) = \sigma_\parallel - \Delta\sigma \cos^2\varphi$.

We can then invert the conductivity matrixto obtain the resistivity matrix $\rho = \sigma^{-1} = \begin{pmatrix} \rho_{xx} & \rho_{xy} \\ \rho_{yx} & \rho_{yy} \end{pmatrix}$, with

$$
\begin{aligned}
\rho_{xx} &= \frac{\sigma_{yy}}{\sigma_{xx}.\sigma_{yy} - \sigma_{xy}^2} = \frac{\sigma_{yy}}{\sigma_\perp . \sigma_\parallel}, \\
\rho_{xy} &= \frac{-\sigma_{xy}}{\sigma_{xx}.\sigma_{yy} - \sigma_{xy}^2} = \frac{-\sigma_{xy}}{\sigma_\perp . \sigma_\parallel} = \rho_{yx}
\end{aligned}
\tag{2}
$$

From Equation 2, we recover the shape of the resistivity from [2]:

$$
\begin{aligned}
\rho_{xx}(\varphi) &= \rho_\perp - \Delta\rho \cos^2\varphi, \\
\rho_{yx}(\varphi) &= \Delta\rho \cos\varphi \sin\varphi,
\end{aligned}
\tag{3}
$$

with $\Delta\rho = \rho_\perp - \rho_\parallel$, $\rho_\perp = 1/\sigma_\parallel$ and $\rho_\parallel = 1/\sigma_\perp$.

However, while the amplitude of the oscillations in conductivity $\Delta\sigma \propto B^2$ is quadratic in field, this is only true at low field for the resistivity:

$$
\Delta\rho = \frac{\sigma_\perp - \sigma_\parallel}{\sigma_\perp \cdot \sigma_\parallel} = -\frac{1}{\sigma_D} \cdot \frac{a/\sigma_D \cdot B^2}{1 + a/\sigma_D \cdot B^2}.
\tag{4}
$$
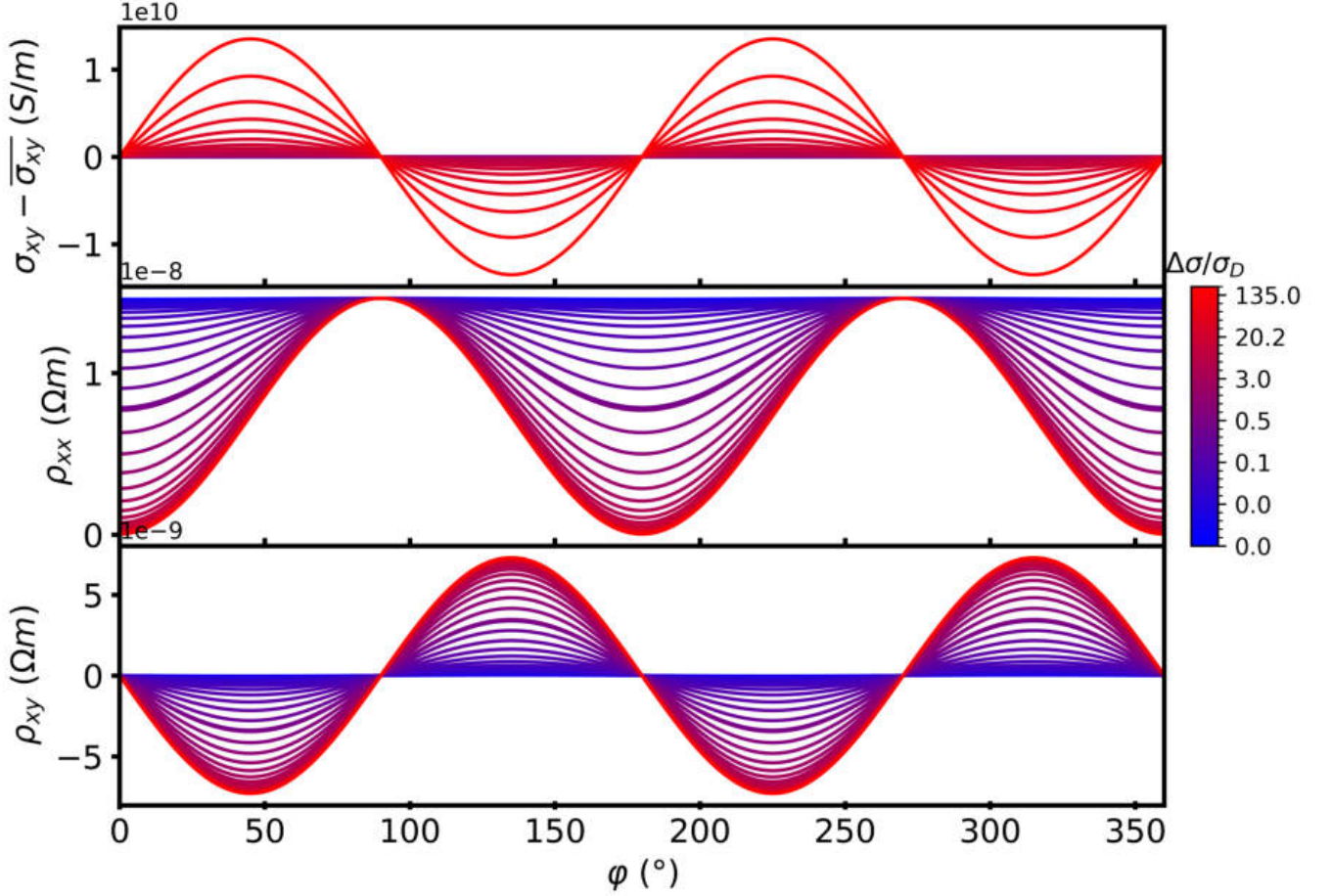
FIG. 1. Simulations showing the angular dependence of the PHE signal in the transverse conductivity (top, vertically offset for visibility), the longitudinal resistivity (middle) and transverse resistivity (bottom), at different magnetic fields from 0.1T (blue) to 300T (red). The corresponding ratio $\Delta\sigma/\sigma_D$ are shown on the right. The parameters used in these simulations are given in section

When $a \cdot B^2/\sigma_D << 1$, we recover the field dependence from [2], $\Delta\rho \propto B^2$, but when $a \cdot B^2/\sigma_D \sim 1$, or alternatively, when $\Delta\sigma \sim \sigma_D$, this approximation breaks down and the oscillations in resistivity begin saturating.

We can estimate at which magnetic field we would expect to see this saturation behaviour in our samples, for instance in $D2$. We can consider that $\sigma_D = 1/\rho_\perp(0T) = 1/R_{xx}(0T) * \dfrac{l}{A}$, with l the distance between the longitudinal contacts, and $A = w * t$, with w, t the width and thickness of the sample, respectively. As a rough estimate, we can take $R_{xx}(0T) \sim 0.836$ Ω, $l \sim 20$ μm, $w \sim 5$ μm and $t \sim 70$ nm, which gives $\sigma_D \sim 6.835$ S/m. In order to get $\Delta\rho(14T) = 387$ $m\Omega * \dfrac{l}{A} \sim 6.7e^{-9}$ Ωm, we choose $a = 3e^5$ S/m in the quadratic field-dependence of $\sigma_\parallel$. The field dependence of the PHE predicted with these parameters is shown in Figure 1 and Figure 2 until 300T.

As expected, the oscillations in resistivity remain sinusoidal over the entire field range, and their amplitude saturates at high field. At low field (i.e. $B < 14$ T), we can fit $\Delta\rho$ well with a subquadratic power law: $\Delta\rho(B) \sim b * B^c$, with $b \sim 1.35e^{-10}$ Ωm and $c \sim 1.50$, which is close to the value obtained in our measurements. Although this model is quite simple, as it assumes a simple quadratic field dependence of $\Delta\sigma$ (as in the pure chiral anomaly case in type-I Weyl semimetals), we can see that 14T is close to the inflection point of the field dependence. Even if the field dependence of $\Delta\sigma$ is slightly slower (i.e. subquadratic), measurements in high-field facilities (e.g. up to 60-100T) should show the saturation. One interesting thing to note is that samples with lower resistivities (i.e. higher conductivities) should show a saturation at higher fields than samples with higher resistivities.
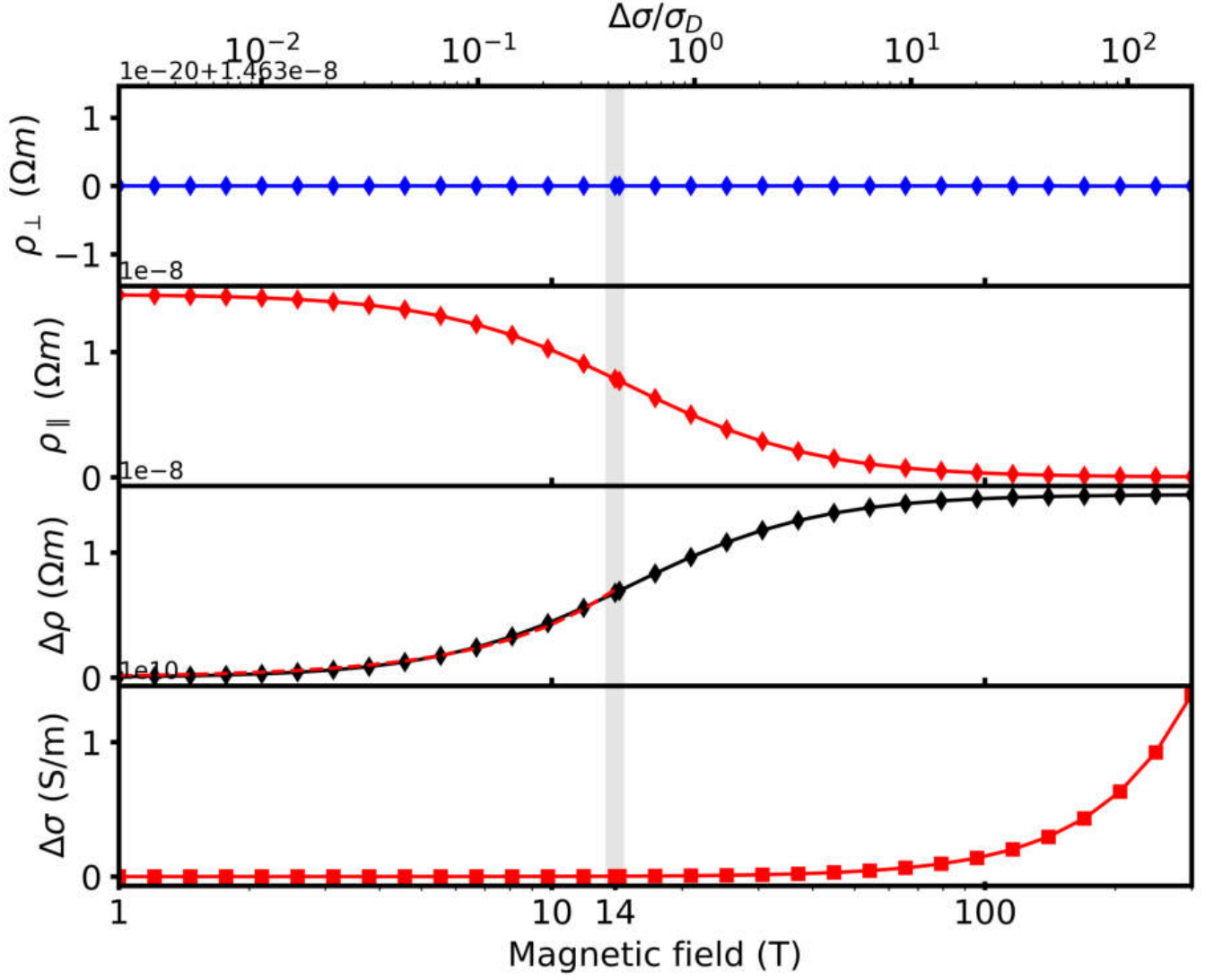
FIG. 2. Field dependence of different parameters of the PHE obtained from fitting the simulations of Figure 1 with Equation 3. The power fit of $\Delta\rho$ is shown in dashed red. The ratio $\Delta\sigma/\sigma_D$ corresponding to the magnetic field is shown at the top. The vertical grey line indicates a magnetic field of 14T.

Discussion on the relative contributions to the PHE

As mentioned in the main text, detailed DFT calculations [3] have found the existence of 3 additional groups of 12 (each) symmetry-related Weyl nodes at high energies, at ~ 141 meV, ~ 300 meV and ~ 320 meV above E_F respectively. In the following, these 4 groups are referred to as the "zero-field" Weyl nodes, as they exist even in the absence of an external magnetic field. Furthermore, these recent calculations also reveal the existence of topological nodal lines - 1D continuous band touchings - in the band structure between the HOMO and LUMO bands (see [3], SM). When a mirror symmetry-breaking magnetic field is applied, these nodal lines convert into a total of 6 additional groups of 6 Weyl nodes (each) along the nodal lines and at various energies (at ~ -655 meV, ~ -497 meV, ~ -80 meV, ~ 202 meV, ~ 285 meV, and ~ 320 meV with respect to E_F), giving rise to an anomalous planar Hall effect (APHE), which we studied in details in [3]. In the following, these 6 groups are referred to as the "field-generated" Weyl nodes, as they only appear when an external magnetic field is applied.

It is extremely difficult to quantitatively differentiate the contributions to the PHE of each groups of Weyl nodes. It can reasonably be assumed that, out of the four groups of zero-field Weyl nodes, the one closest to the Fermi energy (G3 in [4], first predicted in [4]) will contribute the most. Indeed, the contribution of the chiral anomaly to the PHE
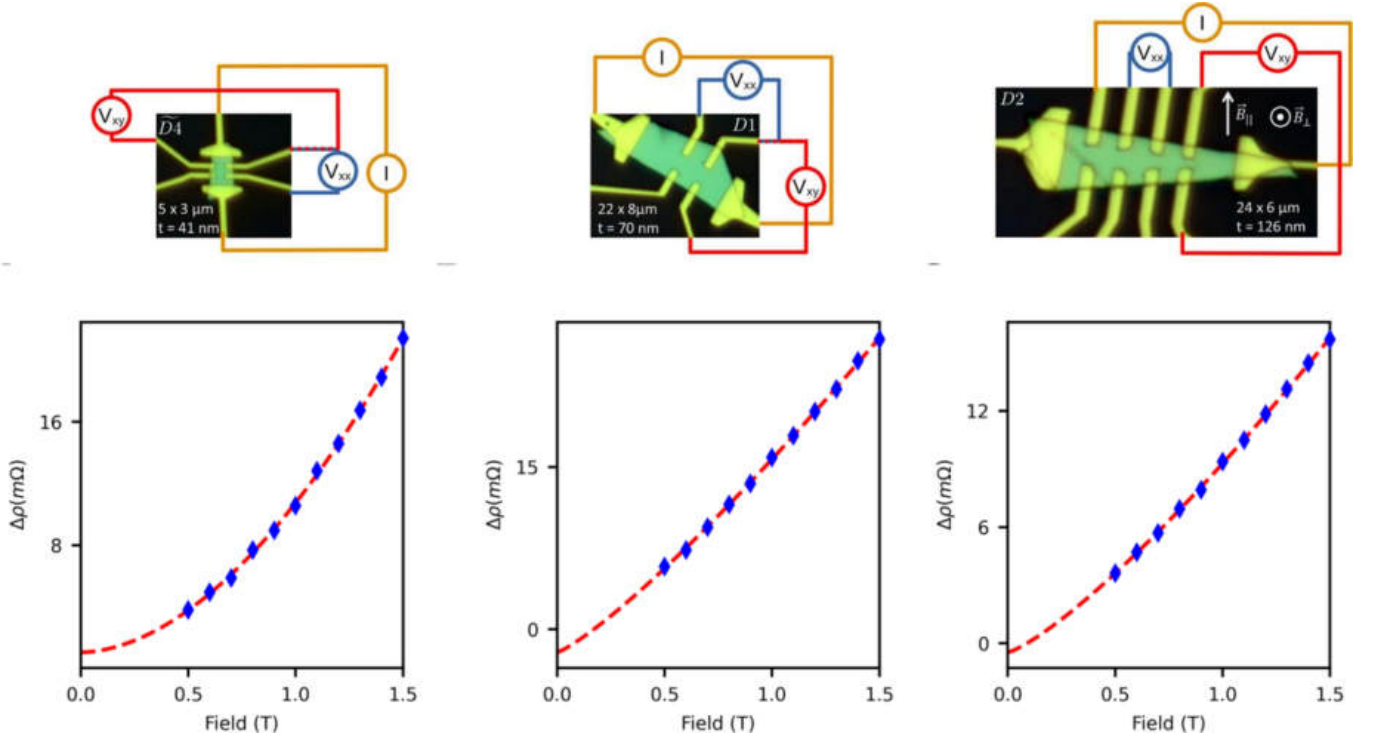
FIG. 3. **a,b,c**: Optical pictures and sample configurations for D3 (41 nm), D1 (70 nm) and D2 (126 nm). The measurements related to each sample is shown below it. **d,e,f**: Amplitudes of the π-periodic oscillations extracted from (d,e,f), for both longitudinal and transverse resistances, at various magnetic fields between 0.5 T and 1.5 T, and their field dependences are fitted to power laws (dashed lines).

comes from the accumulation of carriers around one Weyl cone with a given chirality, and a corresponding depletion of carriers around a Weyl cone with the opposite chirality [5]. When the Fermi energy exceeds the Lifshitz-transition energy, inter-cone scattering will tend to reduce this imbalance in chiral carriers. With WN close in k-space, such inter-cone scattering will occur via long-range disorder, and may therefore be very efficient. This suggests a stronger contribution to the PHE from the Weyl nodes closest to E_F. However, when the WN are far in k-space, the main mechanism behind inter-cone scattering will be due to short-range disorder, which might be far less efficient. As the k-space distance between the field-generated Weyl nodes (from the nodal lines, see [3]) is unusually large (by the very nature of their creation mechanism), we cannot dismiss the contribution of these field-generated Weyl nodes simply due to their distance to the Fermi energy. On the other hand, as the strength of the PHE grows with the square of the Fermi velocity of the Weyl cones [2], one could speculate that, at least in the weak field limit, the zero-field Weyl nodes should give a stronger contribution to the PHE than the Weyl nodes due to conversion of nodal lines, as one could naively expect the Fermi velocity of these field-generated nodes to be roughly proportional to the magnetic field to recover line degeneracies in the $B \to 0$ limit. Therefore, the field-generated Weyl nodes might not contribute much to the PHE. Further research is therefore needed to determine the relative contribution of the different Weyl nodes in this system.

Reproduced from previous publications on the same devices

[*] arthur.veyrat@universite-paris-saclay.fr

[†] cortix@unisa.it

[‡] j.dufouleur@ifw-dresden.de

[1] S. Nandy, G. Sharma, A. Taraphder, and S. Tewari, Physical Review Letters **119**, 1 (2017).
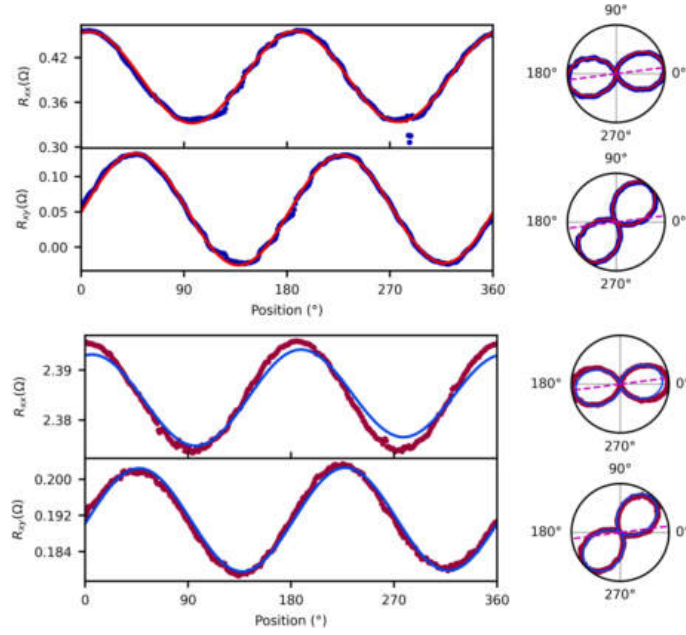
FIG. 4. **a,c**: Angular dependence at 14 T and 1.9 K (a) and 200 K (c) of the longitudinal (R_{xx}, top panels) and transverse (R_{yx}, bottom panels) resistances for sample D2, in Cartesian coordinates. Fits to the PHE model are shown in red (a) and blue (c). **b,d**: Same data as in **a,c**, in polar coordinates. The dashed-line represents the orientation of the current estimated from the data.

[2] A. A. Burkov, Physical Review B **96**, 041110 (2017).

[3] A. Veyrat, K. Koepernik, L. Veyrat, G. Shipunov, I. Kovalchuk, S. Aswartham, J. Qu, A. Kumar, M. Ceccardi, F. Caglieris, N. Pérez, R. Giraud, B. Büchner, J. van den Brink, C. Ortix, and J. Dufouleur, Nature Communications **16**, 6711 (2025).

[4] A. Veyrat, V. Labracherie, D. L. Bashlakov, F. Caglieris, J. I. Facio, G. Shipunov, T. Charvin, R. Acharya, Y. Naidyuk, R. Giraud, J. van den Brink, B. Büchner, C. Hess, S. Aswartham, and J. Dufouleur, Nano Lett. 10.1021/acs.nanolett.2c04297 (2023).

[5] D. T. Son and B. Z. Spivak, Physical Review B - Condensed Matter and Materials Physics **88**, 1 (2013), arXiv:1206.1627.
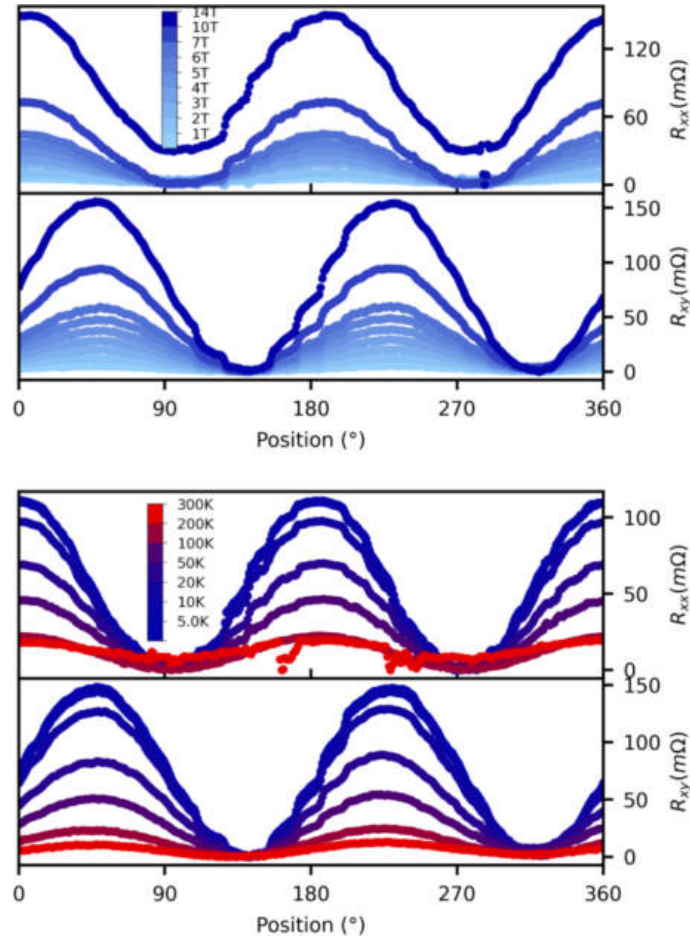
FIG. 5. **a**: Angular dependence of the longitudinal (R_{xx}, top panels) and transverse (R_{yx}, bottom panels) resistances of sample2 D2 at 5K and multiple fields from 1T to 14T. The plots are shifted vertically for visibility, to share a minimum at 0 Ω. **b**: Same as in **a**, for data taken at 14T and at multiple temperatures from 5K to 300K. The plots are shifted vertically for visibility, to share a minimum at 0 Ω.
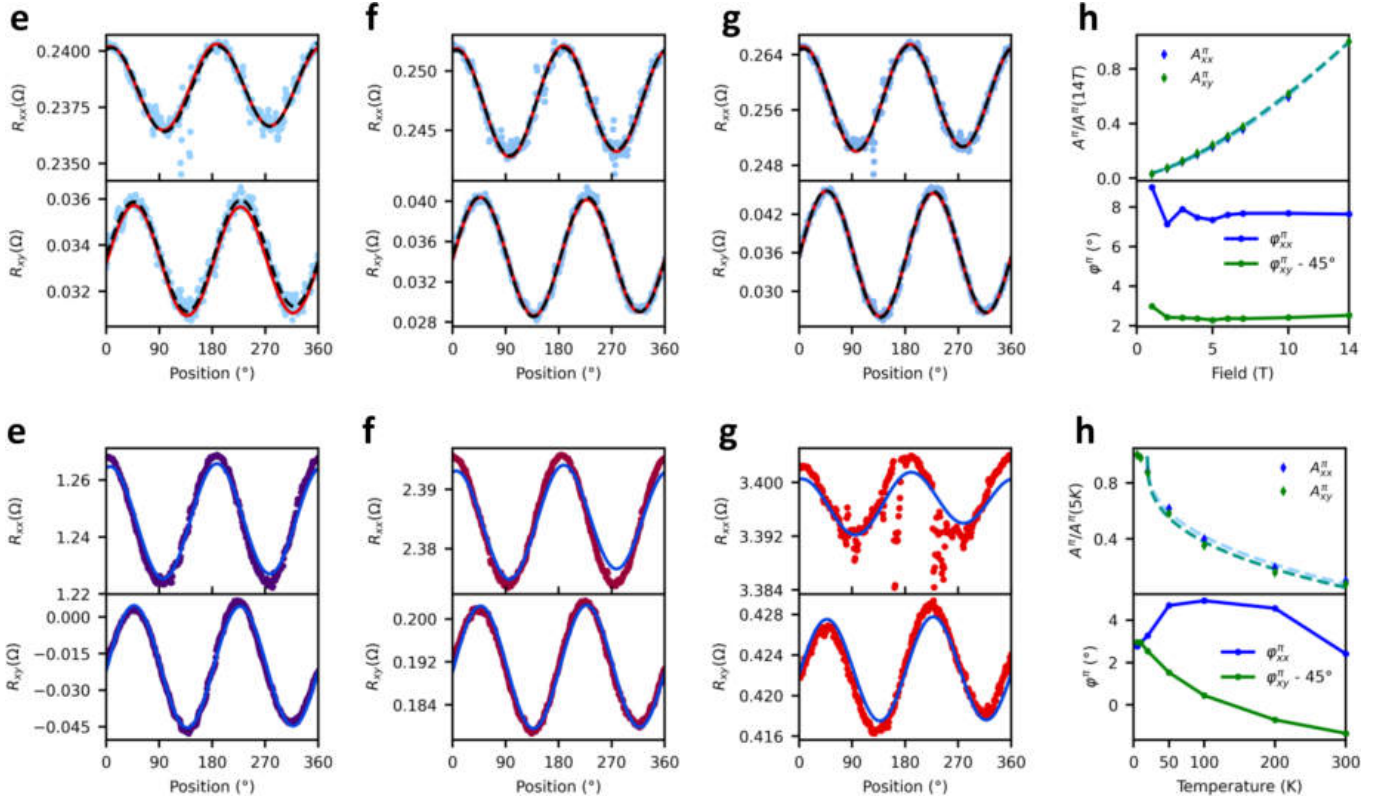
FIG. 6. **a,b,c**: Angular dependence of the longitudinal (R_{xx}, top panels) and transverse (R_{yx}, bottom panels) resistances of sample $D2$ at 1.9 K and 1T (a), 2T (b) and 3T (c). as the variation of the phase and the offset are significantly reduced compared to $D1$, the constrained fits of the PHE model (in red) doesn't deviate as much from the measurements at low fields. The data can be fitted very well with an unconstrained π-periodic fit (in dashed black). **d**: Field dependence of the amplitude (top panel, renormalized to its value at 14T) and phase (bottom panel) of the unconstrained fits of the longitudinal (R_{xx}, blue) and transverse (R_{yx}, green) resistances of $D2$. The renormalized amplitudes of the oscillations in R_{xx} and R_{yx} have the same field dependence, as expected for the PHE. The phase does not vary much in field, with an offset of about $45° + 6°$ between φ_{xx}^{ϕ} and φ_{yx}^{ϕ}. **e,f,g**: Angular dependence of the longitudinal (R_{xx}, top panels) and transverse (R_{yx}, bottom panels) resistances at 14 T and 100 K (e), 200 K (f) and 300 K (g) for $D2$. The constrained fits of the PHE model (in blue) start deviating from the measurements in R_{xx} at high temperature, as the amplitude of the oscillations are smaller than anticipated from those in R_{yx}, just as in $D1$. The data can still be fitted very well with an unconstrained π-periodic fit (in dashed black). **h**: Temperature dependence of the amplitude (top panel, renormalized to its value at 5 K) and phase (bottom panel) of the unconstrained fits of the longitudinal (R_{xx}, blue) and transverse (R_{yx}, green) resistances for $D2$. The renormalized amplitudes of the oscillations in R_{xx} and R_{yx} have a different dependence in temperature, as the amplitude in R_{xx} decreases more slowly than that in R_{yx}. The phase of the oscillations changes slightly with the temperature.
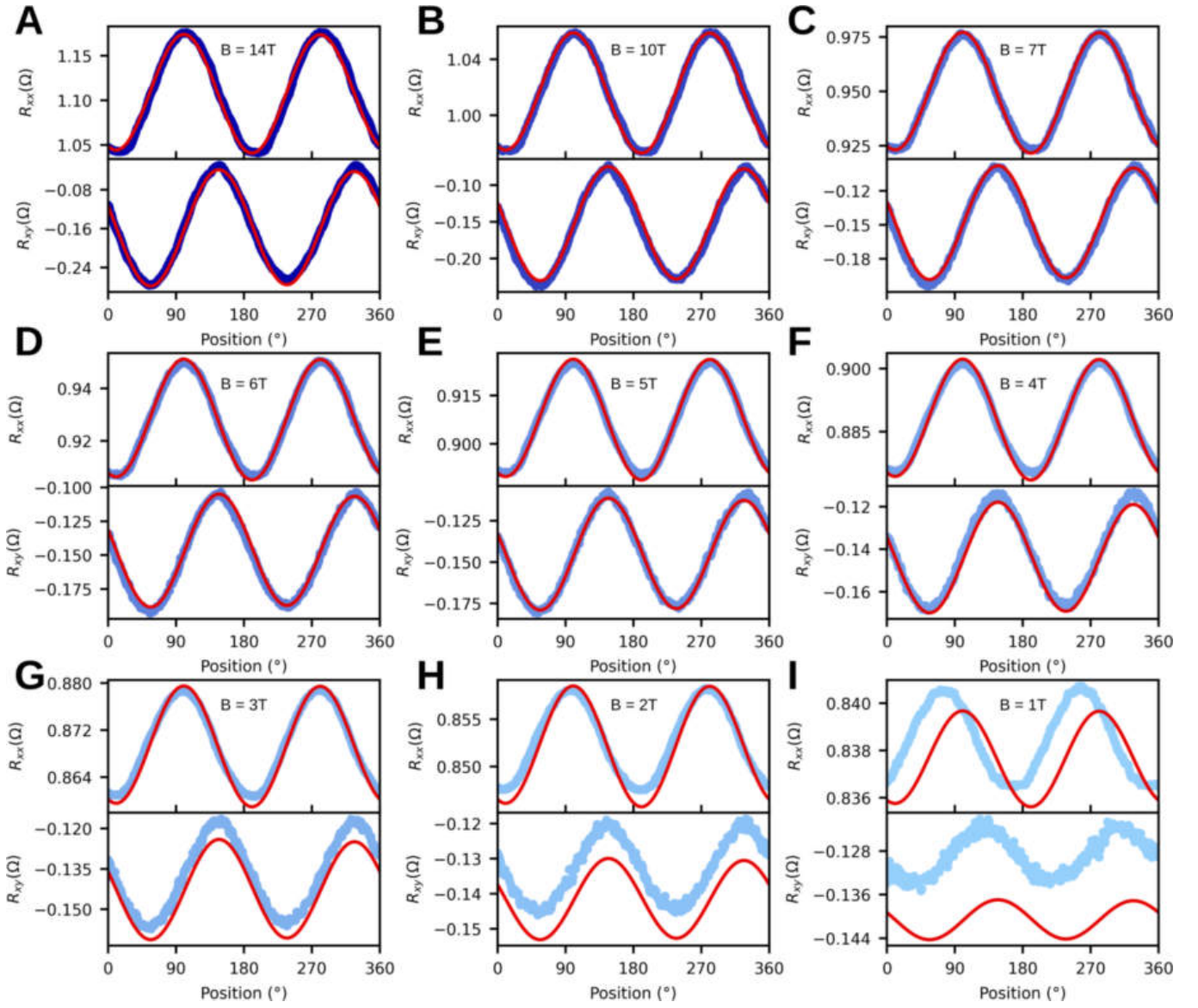
FIG. 7. Raw data: angular dependence of the resistance at different magnetic fields from 1T to 14T for sample D1, at T=5K. The red lines show the fits to the PHE model.
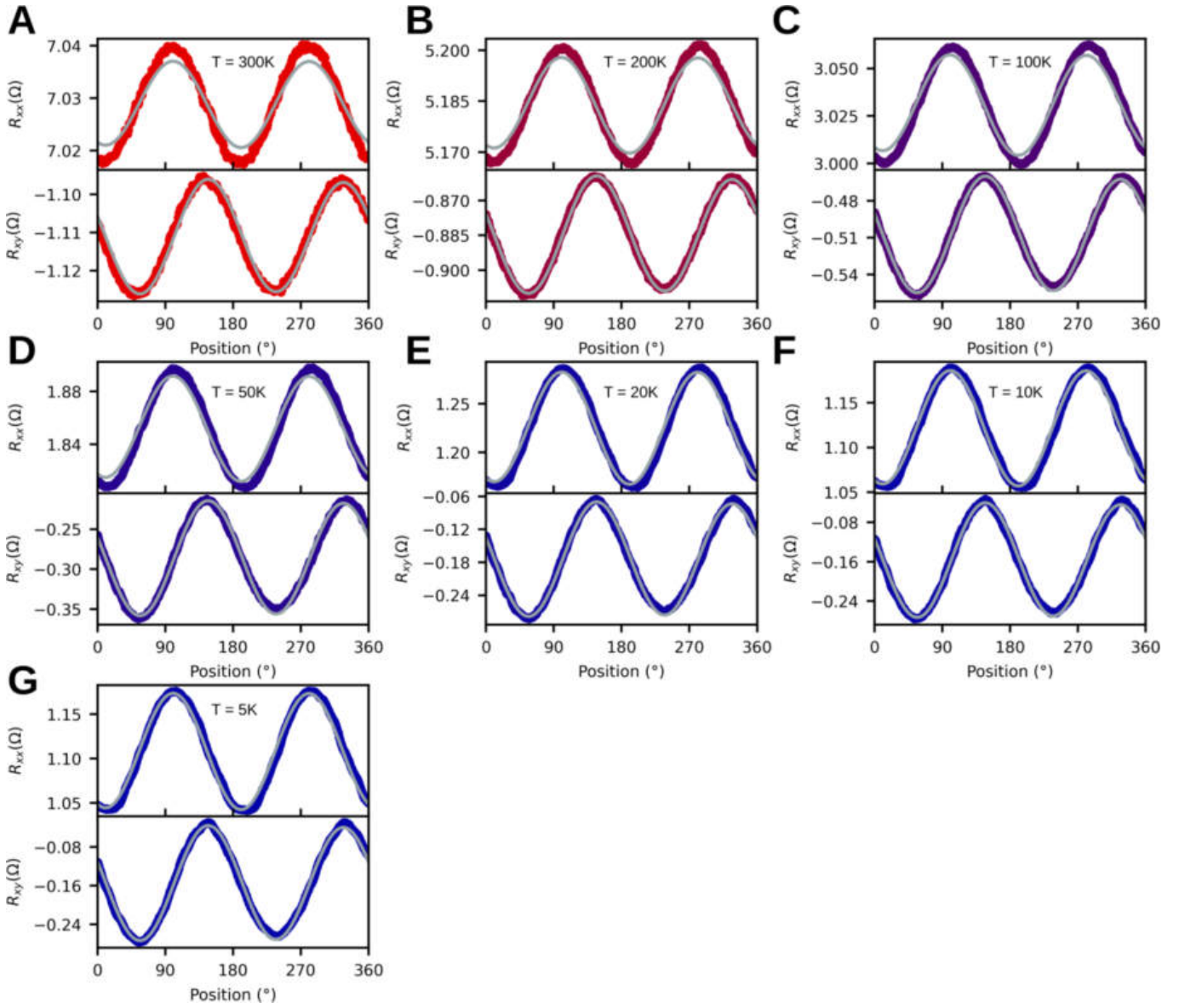
FIG. 8. Raw data: angular dependence of the resistance at different temperatures from 5K to 300K for sample D1, at B=14T. The grey lines show the fits to the PHE model.
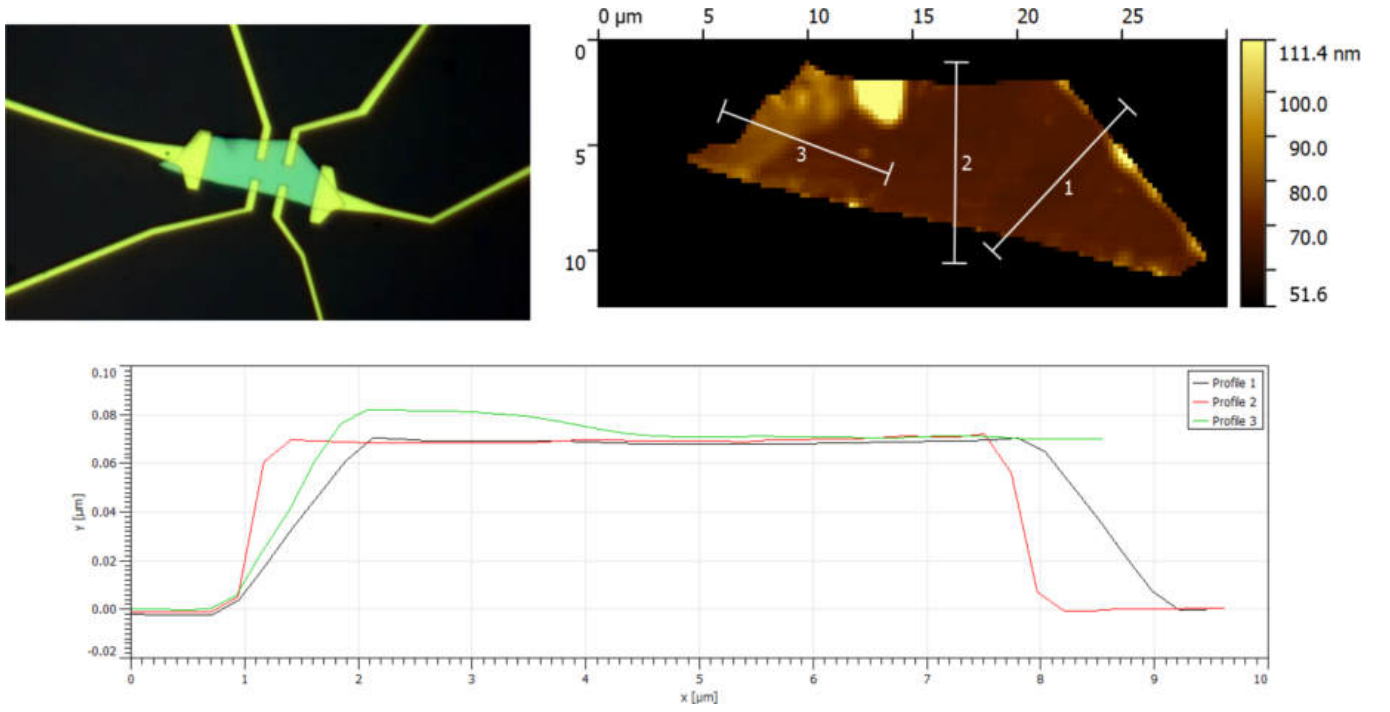
FIG. 9. Optical picture (top left), AFM image (top right) and corresponding profile cuts (bottom) for sample $D1$. The saturated yellow patch probably corresponds to glue residue under (top left) or above (right side) the sample. The flake is shown to be flat over most of its surface, in between the current leads.
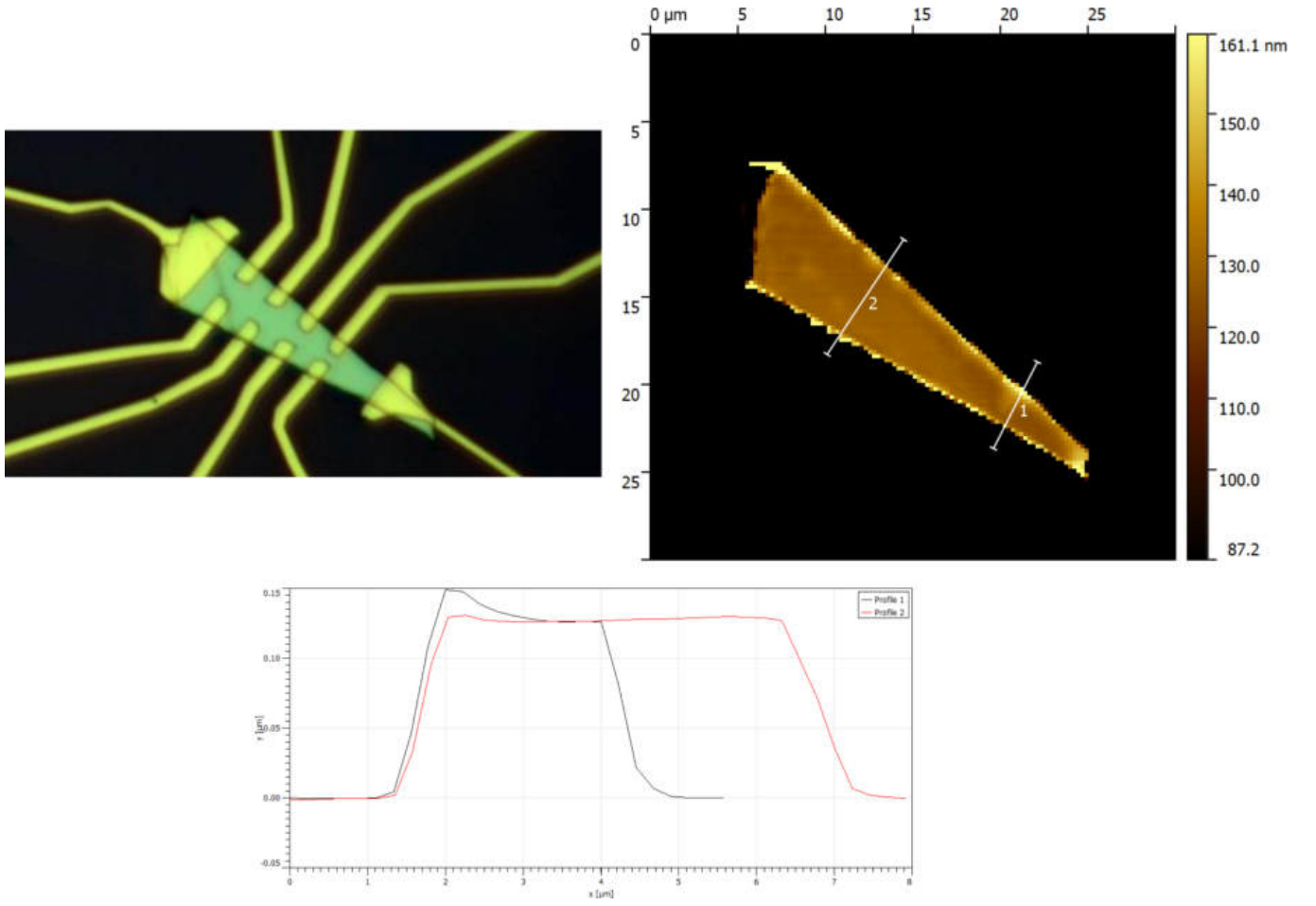
FIG. 10. Optical picture (top left), AFM image (top right) and corresponding profile cuts (bottom) for sample $D2$. The saturated yellow patches probably correspond to glue residue on the edges of the sample. The flake is shown to be flat over most of its surface, in between the current leads.
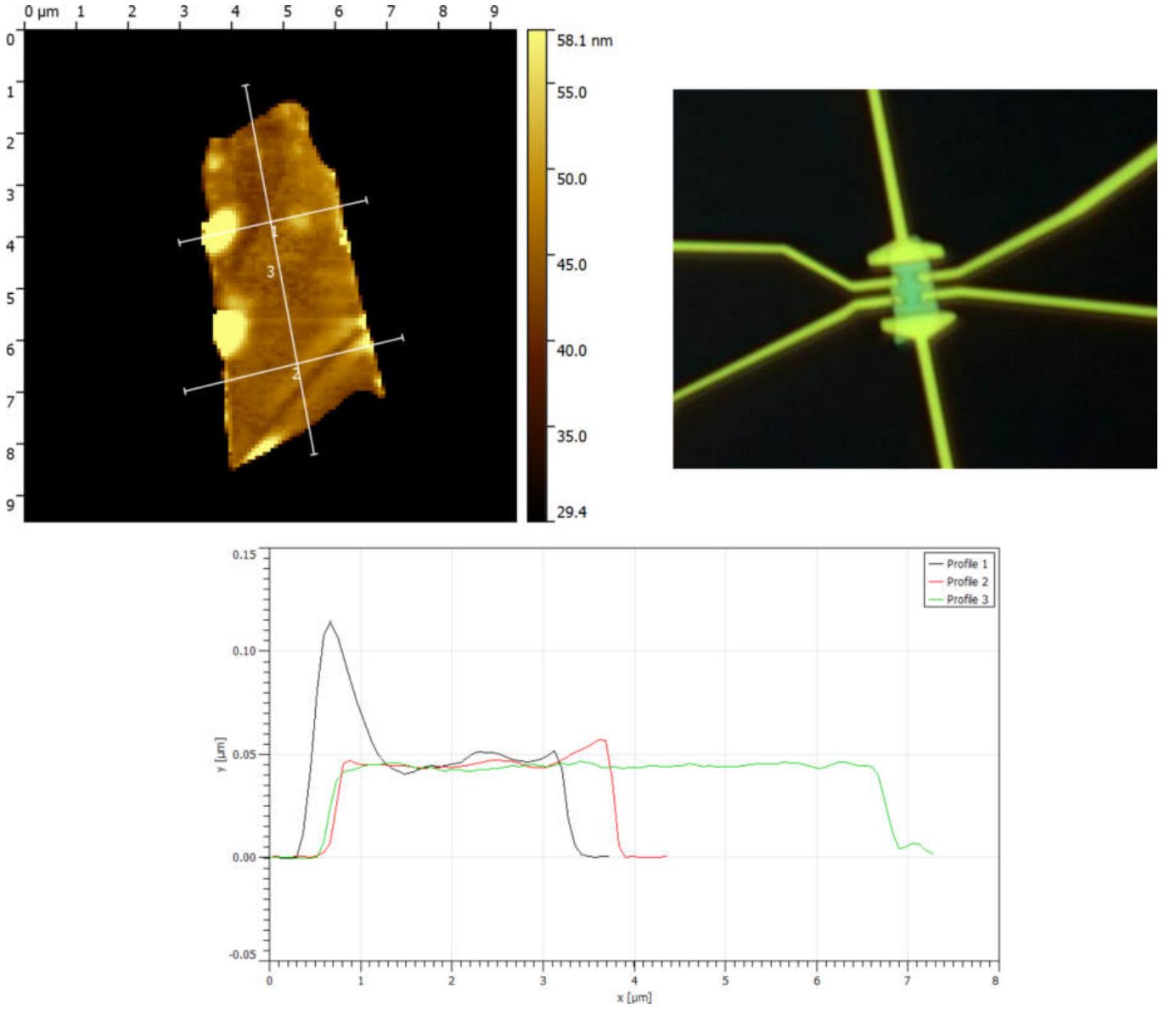
FIG. 11. Optical picture (top left), AFM image (top right) and corresponding profile cuts (bottom) for sample $D4$. The saturated yellow patch probably corresponds to glue residue under (left side) or above the sample. The flake is shown to be flat over most of its surface, in between the current leads.
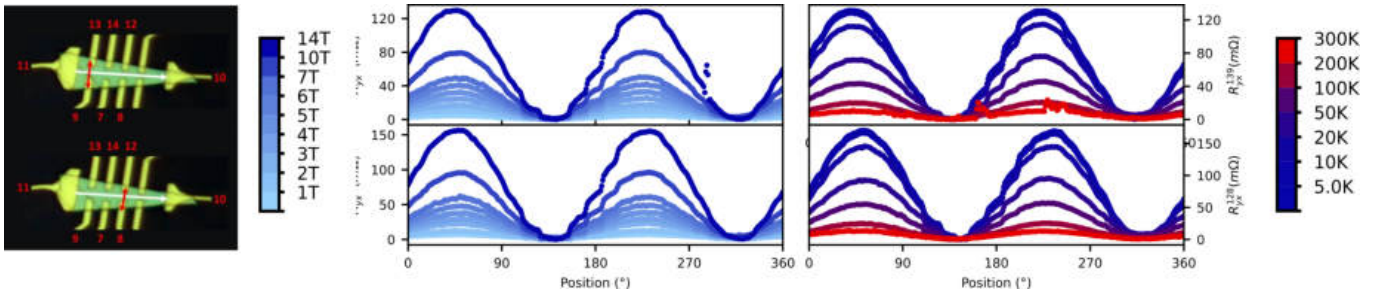
FIG. 12. Transverse resistance measured on sample $D2$ for different contact configurations (shown on the left side, with current direction in white and transverse contacts shown in red. The graphs on the left show the transverse resistance at different fields between 1T and 14T at 1.9K, while the graphs on the right side show the transverse resistance at different temperatures between 5K and 300K at 14T. The color scales are shown on the left side (for the fields) and right side (for the temperatures), respectively.
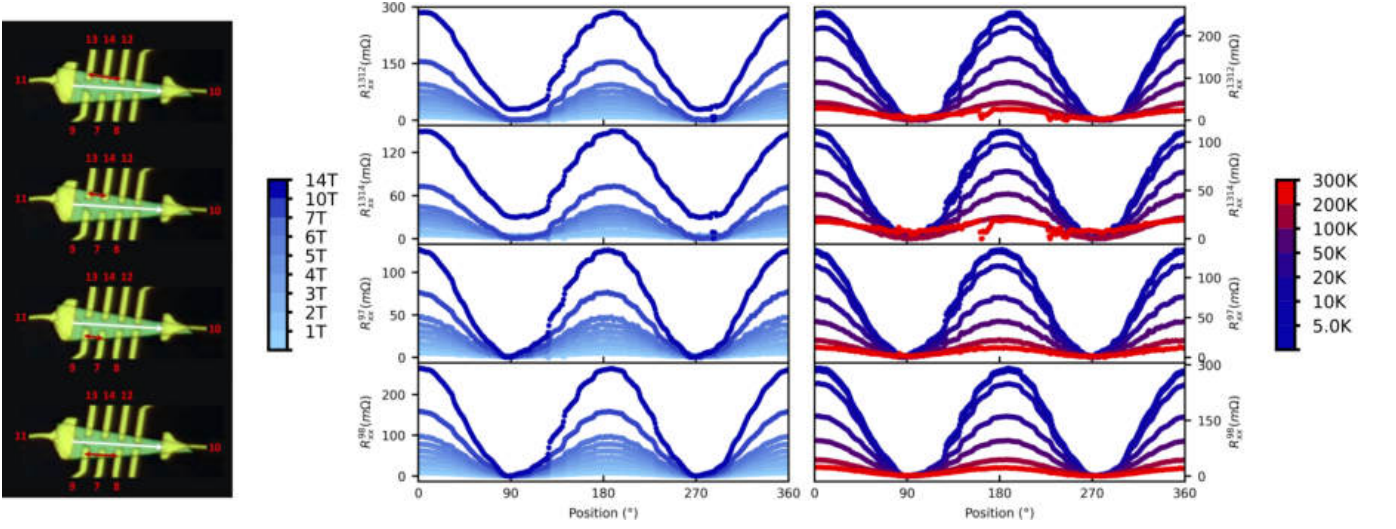
FIG. 13. Longitudinal resistance measured on sample $D2$ for different contact configurations (shown on the left side, with current direction in white and Longitudinal contacts shown in purple. The graphs on the left show the Longitudinal resistance at different fields between 1T and 14T at 1.9K, while the graphs on the right side show the Longitudinal resistance at different temperatures between 5K and 300K at 14T. The color scales are shown on the left side (for the fields) and right side (for the temperatures), respectively.
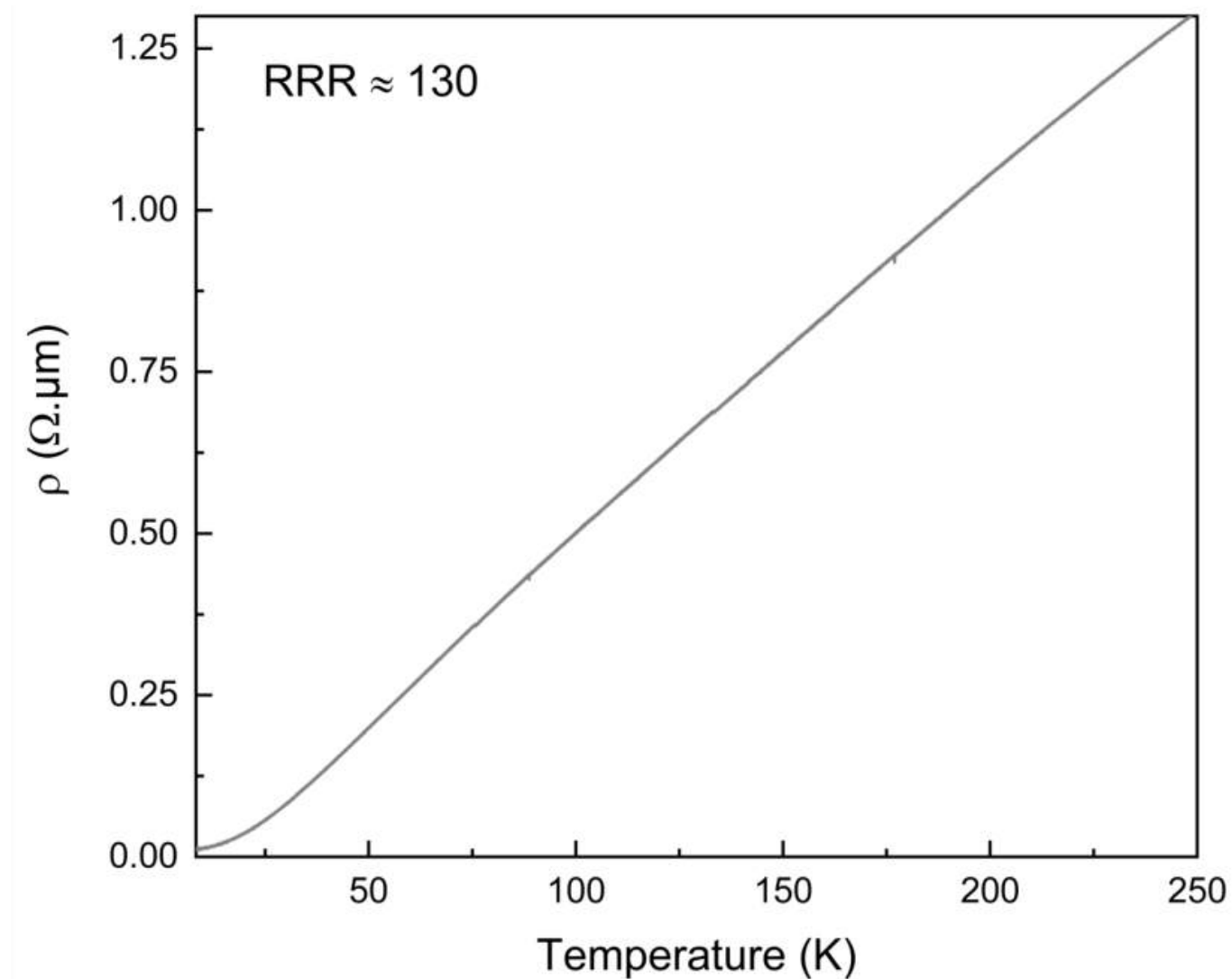
FIG. 14. Temperature dependence of the resistivity of a macroscopic crystal between $T = 300$ K and $T = 4.2$ K. **Reprinted with permission from Veyrat et al. Nano Lett. 2023, 23, 4, 1229–1235. Copyright 2025 American Chemical Society**.
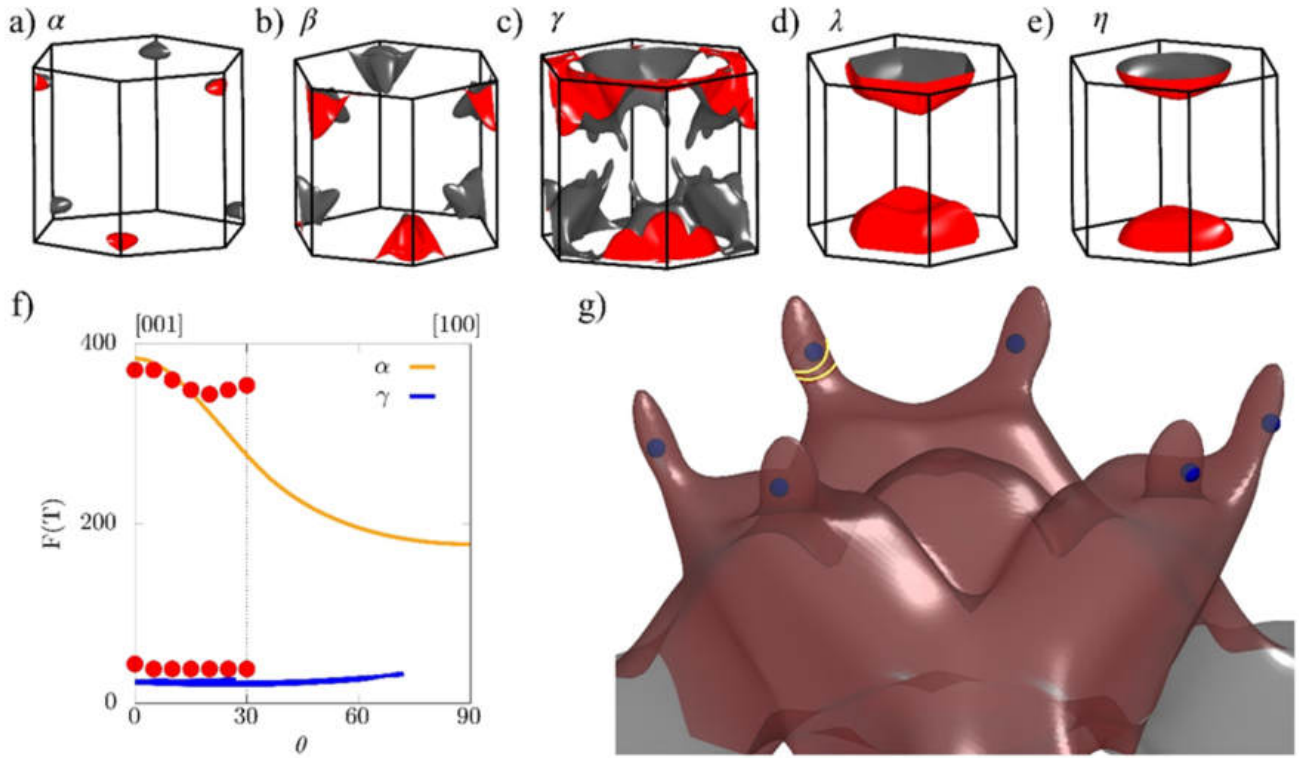
FIG. 15. (a-e) Fermi surface as obtained from density-functional calculations. The outer (inner) face is colored gray (red). (f) Computed quantum-oscillations spectrum at low frequencies. Red points correspond to our experimental results. (f) Extended view of the Fermi surface γ. Weyl nodes are shown as blue points and characteristic extremal orbits of the lowest frequency branch as yellow curves. **Reprinted with permission from Veyrat et al. Nano Lett. 2023, 23, 4, 1229–1235. Copyright 2025 American Chemical Society**.
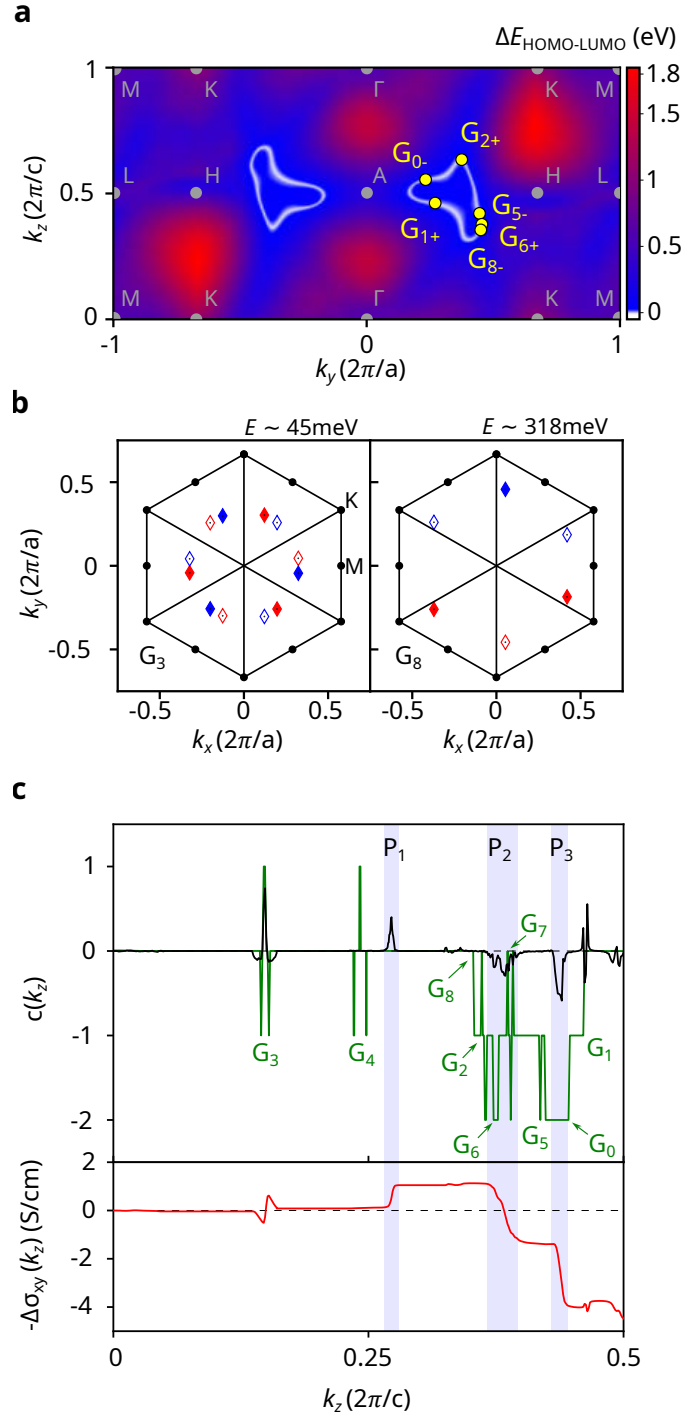
FIG. 16. **Nodal lines and the origin of the anomalous Planar Hall effect in PtBi$_2$**. **a**: Energy gap ΔE between HOMO and LUMO bands in the k_y, k_z (mirror) plane. The nodal loops ($\Delta E = 0$) appear in white. When $B \neq 0$, each nodal loop splits into 6 Weyl nodes (WN, yellow points), forming 6 groups of 6-WN. The signs denote the chiralities. **b**: Two groups of WN of HOMO-LUMO for a Zeeman energy $E_Z = 14$ meV: G_3 is the 12-fold set of WNs closest to E_F already present at $B = 0$, and G_8 is one of the six 6-fold groups mentioned above. The average energies of the groups are shown. Red (blue) markers denotes positive (negative) chirality, while full (empty) markers denote the positive (negative) k_z position of the WN ($G_3 : k_z \sim \pm 0.149$, $G_8 : k_z \sim \pm 0.358$). Solid lines represent the mirror planes, while the dots show the high-symmetry points. **c**: (Top) Chern number $c(k_z)$ in an ideal (green, full HOMO) and a more realistic (black, $E_F = E_{G_3} = 45.3$ meV) case, with a a Zeeman energy $E_Z = 14$ meV. In the ideal case, the Chern number jumps discretely by ± 1 at each WN, while the variation is smoothed out in the realistic case. (Bottom) Anomalous Hall conductivity $-\Delta\sigma_{xy}(k_z)$ calculated from the Chern signal in the realistic case (in black above). The 12 WNs from G_3 at low k_z contribute very little to the AHC, as the Berry curvature they generate is nearly compensated. Most of the AHC comes from 2 peaks in the Chern number at higher k_z, P_2 and P_3 (shown in blue). A third peak at lower k_z, P_1, attenuates the total AHC amplitude, and is found to correspond to WNs from nodal lines below the HOMO band (see Supplementary materials sec. K). Only the $k_z > 0$ dependences are shown, as $c(k_z)$ is even and $\Delta\sigma_{xy}$ is odd in k_z. **Reprinted with permission from Veyrat et al. Nat Commun 16, 6711 (2025).**
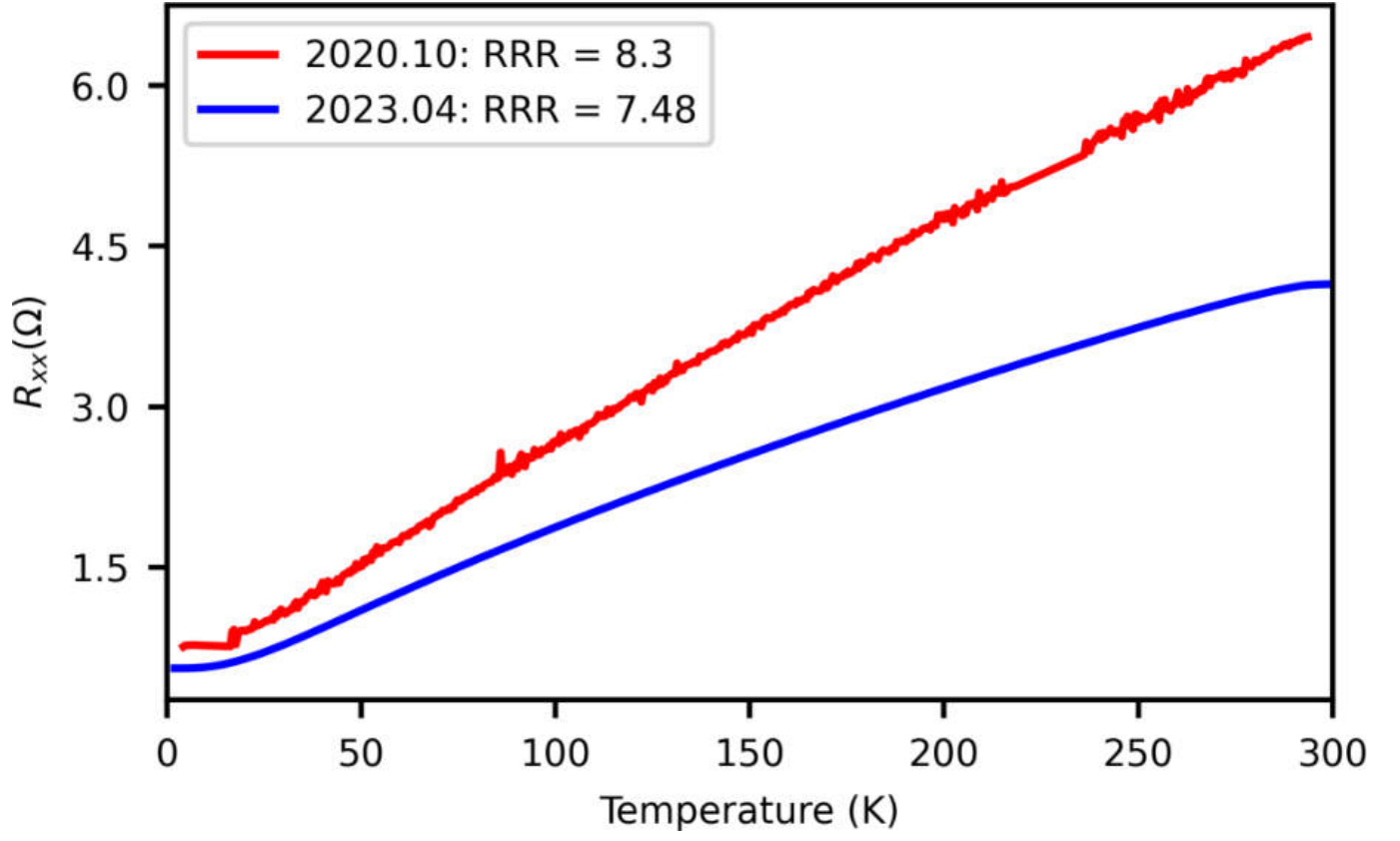
FIG. 17. Comparison of the longitudinal resistance of sample $D1$ between two cooldowns from room temperature to 5K. The residual resistance ration $RRR = \dfrac{R(300K)}{R(5K)}$ is indicated in the inset. **Reprinted with permission from Veyrat et al. Nat Commun 16, 6711 (2025)**.